The Pennsylvania State University

The Graduate School

Department of Meteorology

DEVELOPING THE PENNSYLVANIA STATE UNIVERSITY MEASUREMENT OF OZONE PRODUCTION SENSOR: MOPSv2.0

A Thesis in

Meteorology

by

Bianca C. Baier

Submitted in Partial Fulfillment
of the Requirements
for the Degree of

Master of Science

May 2014

The thesis of Bianca C. Baier was reviewed and approved* by the following:

William H. Brune
Distinguished Professor of Meteorology
Head of the Department of Meteorology
Thesis Adviser

Jerry Y. Harrington
Associate Professor of Meteorology

Anne M. Thompson
Adjunct Professor of Meteorology

Johannes Verlinde
Professor of Meteorology
Chair, Graduate Program in Meteorology

*Signatures are on file in the Graduate School

Abstract

Ambient ozone is a well-known pollutant found in or nearby urban areas that can have adverse health effects on humans and the environment. Air chemistry modeling is used to locate ozone sources, to test ozone mitigation strategies, and to forecast high episodes of ambient ozone. However, it is proving difficult to accurately depict ozone production, $P(O_3)$, due to model uncertainties and inconsistencies between modeled and measured species.

Testing of model output and chemical mechanisms can be achieved with the direct comparison to measured $P(O_3)$. The Penn State MOPSv2.0 provides a more qualitative $P(O_3)$ measurement than the MOPSv1.0. Developments to the MOPS improve upon the MOPSv1.0 component limitations, the measurement technique, and the flow through the chambers. Air flow through the chambers is critical; interactions between air sampled at the output of the chambers and chamber walls can add or remove unwanted chemicals from the air. Thus, a great deal of the chamber and flow development aims to reduce the sampling of air that has interacted with the chamber walls. A new design to the MOPS includes the addition of a heating grid, which increases stability in the chambers. The air flow within the chambers has been developed to be much like a sheath flow regime, which aims to deter air sampled at the outlet of the chambers from interacting with the chamber walls. The MOPSv2.0 is now fully automated and includes a highly-efficient NO_2-to-O_3 converter unit that improves upon the MOPSv1.0 converter unit. In addition, photochemical box model characterization of this new version of the MOPS is much more comprehensive than the MOPSv1.0.

Two MOPSv2.0s, MOPS1 and MOPS2, have been designed, built and deployed to Houston, TX during the "Deriving Information on Surface conditions from COlumn and VErtically resolved observations Relevant to Air Quality" (DISCOVER-AQ) field campaign. The MOPSv2.0s retrieved continuous ozone production rate measurements at two locations: Houston, TX, and Smith Point, TX. Measurements of $P(O_3)$ in both locations provide insight into local ozone source locations and ozone production sensitivity regimes, and provide the first calculations of ozone advection rates. MOPSv2.0 measurements of $P(O_3)$ while they were running at the same location provide validation for the use of the MOPSv2.0s in a network setting and insight into possible sources of error in the MOPS measurement.

The results presented in this thesis demonstrate the potential for the MOPSv2.0 measurement to determine where air quality model output and chemical mechanisms succeed and fail, to aid in the design of air quality standards for mitigating ozone pollution and to provide a direct $P(O_3)$ measurement for assimilation into air quality simulation models.

Table of Contents

List of Tables

List of Figures

List of Reactions

Acknowledgments

I would like to thank my adviser, Dr. William Brune, for giving me the opportunity as an undergraduate to engage in atmospheric chemistry research, for his invaluable guidance and support, and for teaching me how to think like a scientist.

Thank you to my committee members: to Dr. Anne Thompson for her unfailing support, mentoring, and encouragement, and to Dr. Jerry Harrington for his enthusiastic encouragement and motivation.

A special thank you to Dr. David Miller for his scientific instruction and motivation, and for his invaluable LabView expertise and help with MOPSv2.0 construction.

Thank you to Dr. Barry Lefer and his University of Houston research group members Dr. Jimmy Flynn and Sergio Alvarez for their help with radiometric and nitrous acid measurements during the DISCOVER-AQ field campaign. Thank you to Hannah Halliday and Dr. Douglas Martins for their assistance and meteorological measurements in Smith Point, TX.

This work was funded in part by NASA's DISCOVER-AQ program as well as NASA Grant NNX12AB84G.

To my friends both far and away, as well as my wonderful family and loved ones: you have given me the unconditional love and support that has provided motivation and has encouraged me to pursue my scientific endeavors. Thank you.

For Mom and Dad

&

Norb and Greta

Chapter 1

Introduction

1.1 Motivation

Ambient ozone (O_3) is a well-known pollutant found mainly in urban areas and their nearby regions. It has adverse health effects on humans, including: decreased pulmonary function, aggravated asthma, increased emergency department visits, and even mortality (Berman et al., 2012). Equally important, ambient air pollution can vary with socioeconomic circumstances. The understanding that the inhabitants of certain locations may not experience environmental equity is a relatively new concept that gained nationwide attention in the late 1980's (Maantay, 2002). Unfortunately, groups with lower socioeconomic status may receive higher exposure to ozone and other harmful pollutants in the atmosphere because they tend to reside in or near urban areas (O'Neill et al., 2003). Ozone also has damaging effects on plants and ecosystems (Baird and Cann, 2008). Thus, understanding ozone's origins and devising mitigation strategies has been a high priority for governments over the past several decades.

Ozone is designated to be a secondary pollutant in that it is not directly emitted, but is produced in the presence of sunlight through reactions with volatile organic compounds (VOCs), and nitrogen oxides (NO_x = NO + NO_2) (Finlayson-Pitts and Pitts, 2000). These ozone precursors are emitted through anthropogenic activities such as fossil fuel combustion – and a wide range of industrial activities – and can also be formed in

the atmosphere through chemical reactions. The lifetime of ozone in the troposphere depends on its loss due to surface deposition and photochemical atmospheric reactions, and can range from days to weeks. During this time, it can be transported across regions or even from one continent to another in four to ten days (Stohl et al., 2002). Both atmospheric chemistry and transport play important roles in the distribution of ozone.

The Environmental Protection Agency's (EPA) Clean Air Act in 1970 was the first United States effort directed toward mitigation techniques of ozone, nitrogen oxides, and volatile organic compounds. Along with initiating the use of chemical models to predict resultant ozone concentrations in areas, and determining regulation strategies for ozone precursors (NO_x and VOCs), the EPA established a national ambient air quality standard (NAAQS) for six criteria pollutants including ozone. The one-hour standard for ozone was limited to 80 parts per billion (ppb) in 1971 and increased to 120 ppb in 1979 before it was revoked. An eight-hour standard for ozone was also developed and set to 80 ppb in 1997. Recently in 2008, this standard for ozone was lowered to 75 ppb. The Clean Air Act has been effective – the nationally averaged eight-hour ozone level has decreased 28 percent from 1980 to 2010. Despite this success, approximately 108 million people live in counties that have not attained these EPA standards (US EPA, 2010).

1.2 Ozone Chemistry

Ozone is formed through photochemical reactions when NO_x and VOCs are emitted into the atmosphere (Seinfeld and Pandis, 2006). Formation is initiated by reactions of VOCs with hydroxyl (OH) radicals, which are molecular fragments that are highly

reactive due to a lone valence electron. These reaction products further react in cycles with NO, ultimately resulting in ozone formation.

Hydroxyl radicals are produced in the atmosphere by the photolysis of several molecules. Most important, is the photolysis of O_3 to produce excited oxygen, ($O(^1D)$), which then reacts with water vapor to produce OH (Reaction 1.1 - Reaction 1.3) (Seinfeld and Pandis, 2006).

$$O_3 + h\nu \longrightarrow O_2 + O(^1D) \quad \{1.1\}$$

$$O + O_2 + M \longrightarrow O_3 + M \quad \{1.2\}$$

$$O(^1D) + H_2O \longrightarrow 2\,OH \quad \{1.3\}$$

The hydroxyl radical can also be formed through photolysis of nitrous acid (HONO) and hydrogen peroxide (H_2O_2). Ozone and oxygen (O_2) are the main oxidizing constituents in the atmosphere. However, their large bond energies inhibit them from reacting with other species, leaving OH as the primary oxidizing agent in the troposphere.

Nitrogen oxides have their own chemical cycle that is independent of the VOC products. In the presence of sunlight, NO_2 photolyzes to form nitric oxide, NO, which recombines with ozone to form NO_2 via Reaction 1.4 - Reaction 1.6. Nitrogen dioxide can then be photolyzed again in a repeatable process known as the NO_x photostationary state (PSS). However, this sequence of reactions produces zero net ozone molecules.

$$NO_2 + h\nu(\lambda < 424\,nm) \longrightarrow NO + O \quad \{1.4\}$$

$$O + O_2 + M \longrightarrow O_3 + M \quad \{1.5\}$$

$$NO + O_3 \longrightarrow NO_2 + O_2 \quad \{1.6\}$$

The reaction of OH with VOCs forms peroxy radicals, which are HO_2 and RO_2, where "R" indicates an organic radical. The reactions of the peroxy radicals with NO ultimately produce new ozone through Reactions 1.7-1.9.

$$VOC + OH \longrightarrow RO_2 + H_2O \quad \{1.7\}$$

$$RO_2 + NO \longrightarrow R'CHO + HO_2 + NO_2 \quad \{1.8\}$$

$$HO_2 + NO \longrightarrow NO_2 + OH \quad \{1.9\}$$

New ozone is formed by this interruption of the NO_x PSS with an additional production of NO_2 as seen in Reactions 1.8 and 1.9. Additional NO_2 (and consequently, ozone) will continue to be formed outside of the NO_x PSS with this HO_x ($OH + HO_2$) and NO_x cycling until peroxy radicals and NO are no longer present (Seinfeld and Pandis, 2006).

Ozone production ceases through the termination of HO_x and NO_x cycling, and is therefore dependent upon NO_x concentrations. If NO_x is high, OH radicals react with NO_x instead of oxidizing VOCs. Reactions 1.10 - 1.11 depict this scenario with the

formation of nitric acid, HNO_3, and organic nitrates via radical- NO_x reactions. For lower NO_x concentrations, and thus higher VOC concentrations, the termination occurs with radical-radical reactions, as in Reaction 1.12, with the formation of hydrogen peroxide (Kleinman, 2005).

$$OH + NO_2 + M \longrightarrow HNO_3 + M \quad \{1.10\}$$

$$RO_2 + NO \longrightarrow \text{products} \quad \{1.11\}$$

$$HO_2 + HO_2 \longrightarrow H_2O_2 + O_2 \quad \{1.12\}$$

As an example, the simplest reaction pathway for ozone formation occurs with methane oxidation, which can react with the hydroxyl radical to ultimately form new NO_2 through Reactions 1.13 - 1.14.

$$CH_4 + OH \longrightarrow CH_3O_2 + H_2O \quad \{1.13\}$$

$$CH_3O_2 + NO \longrightarrow NO_2 + HCHO + HO_2 \quad \{1.14\}$$

The reaction of CH_3O_2 leads to the formation of methyl hydroperoxide in Reaction 1.15, which can either photolyze or react with OH to form formaldehyde (HCHO), a common oxidation product of many hydrocarbons. One pathway from photolysis of formaldehyde can form CO, which can also oxidize to theoretically form one new ozone

molecule. Another pathway in Reaction 1.19 of HCHO photolysis yields to an additional hydroperoxy radical.

$$CH_3O_2 + HO_2 \longrightarrow CH_3OOH + O_2 \quad \{1.15\}$$

$$CH_3OOH + h\nu \longrightarrow CH_3O + OH \quad \{1.16\}$$

$$CH_3OOH + OH \longrightarrow CH_3O_2 + HCHO + OH \quad \{1.17\}$$

$$HCHO + h\nu \longrightarrow CO + H_2 \quad \{1.18\}$$

$$HCHO + h\nu \longrightarrow H + HCO \quad \{1.19\}$$

$$H + O_2 \longrightarrow HO_2 \quad \{1.20\}$$

$$HCO + O_2 \longrightarrow HO_2 + CO \quad \{1.21\}$$

Thus, if each hydroperoxy radical in the above mechanism reacts with NO as in Reaction 1.9, the oxidation of one molecule of methane would produce a total of four nitrogen dioxide molecules and, consequently, four new ozone molecules. Since the oxidation of carbon monoxide, CO, theoretically forms one additional ozone molecule, the total theoretical yield of methane oxidation is five new ozone molecules (Seinfeld and Pandis, 2006).

1.2.1 P(O_3) and NO_x-VOC Sensitivity

The following Equation 1.1 outlines the total chemical production of ozone. The chemical ozone formation is dependent on NO_x and VOCs; a key question for ozone abatement strategies is how ozone formation reacts to changes in these two precursors.

$$p(O_3) = k_{NO+HO_2}[NO][HO_2] + \sum k_{NO+RO_{2i}}[NO][RO_2]_i \quad (1.1)$$

Because NO_x is involved in both the production and the loss of the radicals, and thus the ozone production, ozone production does not depend linearly on NO_x and VOCs over the entire range of concentrations. Two regimes for ozone formation are NO_x-limited and VOC-limited (Kleinman, 2005). Many metrics for determining NO_x-limited (sometimes called NO_x-sensitive) and VOC-limited (or VOC-sensitive) regimes have been defined, as conditions for which ozone production changes due to changes in NO_x or changes in VOCs (Sillman and Samson (1995), Kleinman et al. (1997),Tonnesen and Dennis (2000)). Recent studies (Mao et al. (2010), Ren et al. (2013)) have used the ratio proposed by Kleinman (2005), $\frac{L_N}{Q}$, to evaluate O_3 production sensitivity. Here, L_N is the free radical removal rate due to reactions with NO_x and Q is the total radical production rate. Thus, $\frac{L_N}{Q}$ represents the fraction of free radicals removed from the atmosphere due to reactions with NO_x. The ratio $\frac{L_N}{Q} << 0.5$ represents an atmosphere in a low NO_x or NO_x-limited regime, whereas if $\frac{L_N}{Q}$ is $>> 0.5$ the atmosphere is in a high NO_x, or VOC-limited regime. The quantity $\frac{L_N}{Q}$ is dependent on NO_x, and therefore dependent on the time of day (Ren et al., 2013), so understanding ozone production within NO_x-limited and VOC-limited regimes, and the chemical constraints within these regimes, will help air chemistry models to more accurately portray ozone chemistry. In this way, measuring ozone production can be a first step in regulating ozone in areas of non-compliance.

1.2.2 The Ozone Budget Equation and Ozone Transport

Equation 1.2 shows the local change in ozone over time and its dependence on atmospheric chemistry, surface deposition, and local meteorology.

$$\frac{\partial[O_3]}{\partial t} = p(O_3) - l(O_3) - \frac{u_d}{H}[O_3] - \mathbf{v} \cdot \nabla[O_3] \tag{1.2}$$

Here, the local change in ozone depends on the chemical production of ozone, $p(O_3)$, $l(O_3)$, where

$$l(O_3) = k_{OH+NO_2+M}[OH][NO_2][M] + k_{HO_2+O_3}[HO_2][O_3] + P(RONO_2) \tag{1.3}$$

is the chemical loss of ozone, u_d, the surface deposition velocity, H, the boundary layer height, and $\mathbf{v}$, the wind velocity. Distinguishing which factor contributes to the most ambient ozone can prove to be difficult, as changes in ozone can be due to advection from point sources, mixing to lower levels from residual layers, and local production. The instantaneous ozone production rate, $P(O_3)$, can be summarized by Equation 1.4 where

$$P(O_3) = p(O_3) - l(O_3). \tag{1.4}$$

Measuring the instantaneous ozone production rate, $P(O_3)$, can help to determine whether ozone is produced locally, or advected to any location. By comparing the local change in ozone, $\frac{\partial O_3}{\partial t}$, to ozone production, it is possible to assess ozone advection (assuming all ozone deposition is small). If $\frac{\partial O_3}{\partial t}$ at a measurement site is small, but

$P(O_3)$ is large, then air with less ozone is being advected to the location. Likewise, if $\frac{\partial O_3}{\partial t}$ is large and $P(O_3)$ is small, then it is likely that higher amounts of ozone are being advected to the location. Determining point sources of ozone production and how ozone is vertically and horizontally advected can help air quality models to pinpoint locations where ozone abatement strategies need to be adjusted.

1.3 Ozone Production and Air Quality Simulation Models

Air chemistry modeling is used to locate sources of pollution, to test mitigation strategies before they are enforced, and to predict ozone episodes so that ozone reduction strategies can be implemented. Recently, health fields have been implementing air quality models to locate sources of pollution (Fann et al. (2009), Liu et al. (2007), Zhou et al. (2013)).

Traditionally, ozone has been either predicted by chemical models or calculated if radical abundances are known. However, it is proving difficult to accurately depict ozone production, $P(O_3)$, due to model uncertainties and discrepancies between modeled and measured results.

First, ozone chemistry and model initial conditions have yet to be understood and universally accepted. $P(O_3)$ in NO_x-limited and VOC-limited regimes has yet to be well characterized in Equation 1.1, and it is seen that the local change in ozone can be attributed to a number of variables including the planetary boundary layer height and ozone transport (Equation 1.2). Uncertainties in air quality models include model boundary conditions, heterogeneous chemistry, and description of long-range transport of

ozone and its precursors under various meteorological conditions (Texas Commissionon Environmental Quality, 2010).

Second, modeled versus measured radical abundances are still in disagreement. Models under-predict HO_2 at high NO, and under-predict HO_x (OH + HO_2) at night. A greater understanding of OH-HO_2 cycling at high NO is salient in correctly modeling ozone production (Ren et al., 2013). Additionally, field studies (Olaguer et al. (2013), Ren et al. (2013), Texas Commissionon Environmental Quality (2010)) have noted that model chemical mechanisms may be underestimating radical sources such as HONO and formaldehyde (HCHO), which can therefore underestimate $P(O_3)$.

Third, model chemical mechanisms are still in disagreement. A number of evaluations and comparisons of different models' chemical mechanisms have been conducted (Chen et al. (2010), Derwent (1990), Jimenez et al. (2003), Luecken et al. (2008)). A salient aspect of these air quality simulation models (AQSMs) is the model's chemical mechanism that describes atmospheric gas-phase chemistry and ozone formation. In particular, uncertainty in modeled $P(O_3)$ arises in chemical mechanism reaction rate coefficients and reaction products and can be higher during early morning hours (0600-0900) when $P(O_3)$ is thought to be large (Chen and Brune, 2012). To validate these mechanisms, they must be compared to measurements (Carter and Lurmann, 1991). $P(O_3)$ is one of the few variables in the ozone budget equation that can be independently tested against experimental data.

To determine the validity of these AQSM chemical mechanisms and input, the model results must be compared to either measurements in environmental chambers or in the atmosphere. Until recently, a direct measurement of ozone production has not

been available for such comparisons. Direct $P(O_3)$ measurements can act as a serious constraint on possible chemical mechanisms for ozone production. Understanding the differences between measured and model-derived ozone production can be a first step in understanding ozone chemistry and validating air chemistry models.

A direct measurement of $P(O_3)$ can also be useful in improving chemical transport models and accurately forecasting ozone. Because meteorological time scales are much longer than the time scales of atmospheric processes, pertinent information can be lost between model outputs. Assimilating $P(O_3)$ in AQSMs can help to guide the model chemistry in the same manner that meteorological data helps to guide weather forecasts.

If direct measurements of $P(O_3)$ can be assimilated into AQSMs such as the Weather Research and Forecasting (WRF) model, it may allow for a more accurate prediction of ozone concentrations. As models like WRF are now fully coupled with an "online" chemistry scheme (WRFChem), the air quality component of the model is fully consistent with the meteorological component (Grell et al., 2005). $P(O_3)$ observations combined with numerical results can improve our capability to predict ozone in urban and non-attainment areas, and to locate instances of environmental injustice.

The following chapter outlines the Pennsylvania State University Measurement of Ozone Production Sensor (MOPS), developments to this new instrument (MOPSv2.0), and the instrument's measurement technique. Chapters two and three outline the development of the MOPS measurement process, raw data processing, and calibration techniques, as well as characterization of the instrument, and laboratory results and diagnostics. Chapter four presents field results since these developments, while the final chapter is dedicated to conclusions from the developmental research and field studies

and proposes future renovations and research needed to continue to improve the MOPS $P(O_3)$ measurement.

Chapter 2

Instrumentation

2.1 The Penn State Measurement of Ozone Production Sensor

The Measurement of Ozone Production Sensor (MOPS) directly measures the ozone production rate, $P(O_3)$ (Cazorla and Brune, 2010). This idea of a direct measurement of $P(O_3)$ was first proposed in a Ph.D dissertation by Harvey Jeffries (Jeffries et al., 1976). However, limitations with materials, methods and the understanding of ozone chemistry made it difficult to obtain a quantitative measurement of $P(O_3)$ and the idea was never published in peer-reviewed literature. Unaware of this work, the Penn State University independently came up with the MOPS concept about a decade ago and have used current materials, methods, and knowledge of the chemistry to develop the MOPS, which shows promise for giving quantitative measurements.

The MOPSv1.0 described in Cazorla and Brune (2010) measures $P(O_3)$ by calculating the difference of ozone coming from a transparent, sample chamber and from a reference chamber covered with Ultem® film which blocks all radiation less than 400nm. Hence, the sample chamber mimics the photolytic chemistry of the atmosphere, while the reference chamber blocks all radical chemistry. Since radicals are needed to interrupt the NO_x PSS and create new NO_2, the reference chamber also blocks all ozone production. A NO_2-to-O_3 converter accounts for differences in NO_x PSS between the sample and reference chambers. By measuring the difference of the total $NO_2 + O_3$ between the

chambers (sample - reference), it is possible to cancel the NO_x PSS chemistry, leaving an instantaneous measurement of the new ozone produced. The remaining $NO_2 + O_3$ in the sample and reference chambers is then measured as O_3 in a modified ozone analyzer. A schematic of the MOPSv1.0 is shown in Figure 2.1.

The measurement of new ozone divided by the exposure time, τ, in the chambers gives an instantaneous ozone production rate in parts per billion by volume per hour (ppbv hr^{-1}), as in Equation 2.1.

$$P(O_3) = \frac{\triangle(O_3)}{\tau} \tag{2.1}$$

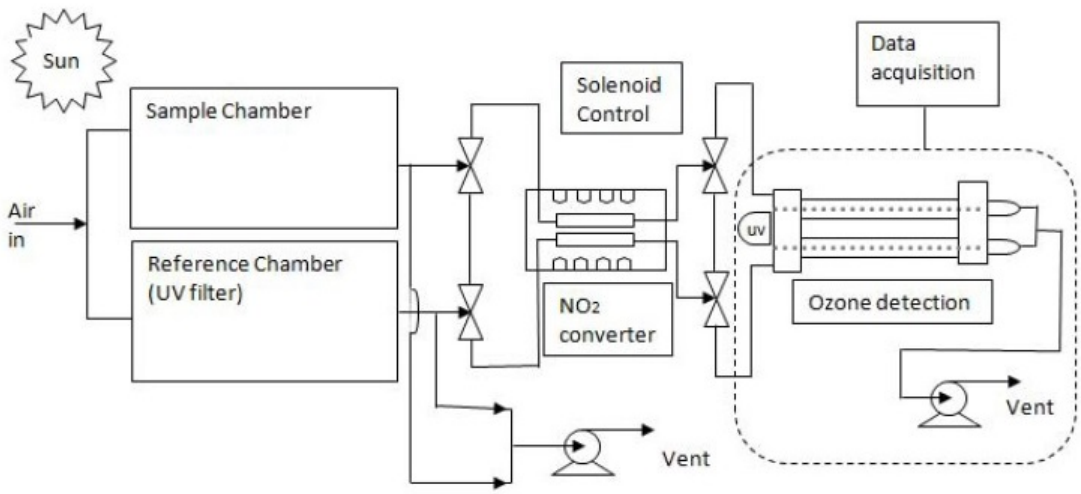

Fig. 2.1. Schematic of MOPSv1.0. Air is sampled continuously through sample chamber and reference chambers. A sample chamber mimics the atmosphere while a reference chamber blocks all UV radiation $<$ 400nm (Cazorla and Brune, 2010).

2.1.1 MOPSv1.0 Field Deployments

One MOPSv1.0 was deployed in Houston, TX during the SHARP field campaign in 2009 (Cazorla et al., 2012). The MOPS sampling site was on the roof of University of Houston's Moody Tower North located 70m above ground level and 5km south of downtown Houston from 15 April 2009 to 31 May 2009. Here, the MOPS direct $P(O_3)$ measurement was compared to calculated ozone production rates via Equation 1.4, using both measured and modeled HO_2, NO, and OH radicals. The SHARP 2009 deployment was the first attempt to use this new instrument to contribute to the understanding of ozone chemistry as discussed in Ren et al. (2013).

The MOPSv1.0 production rates obtained from the 2009 SHARP field campaign also provided a test for calculated $P(O_3)$ versus modeled $P(O_3)$ based on measured HO_2 and OH. These measured $P(O_3)$ rates were found to be similar to calculated $P(O_3)$ rates, but the peak values were shifted to later in the morning. The shape of the diurnal curve was similar to the modeled diurnal curve, but was more than twice as large. Unfortunately, measurement uncertainties prevented the MOPSv1.0 measurements from determining whether the calculated or modeled ozone production rate was correct. Further development to the MOPSv1.0 was needed to reduce or eliminate these uncertainties in this $P(O_3)$ direct measurement (Cazorla et al., 2012).

The MOPSv1.0 was able to capture ozone production rates during the morning hours, but routinely measured negative production rates during the early morning and evening hours. The theoretical explanation for this could be that the ozone removal rate in Equation 1.4 is larger than the production rate, causing a net loss of ozone. Another

explanation for these negative production rate measurements could be due to a chemical loss of ozone on the walls of the MOPSv1.0 chambers. More likely, as discussed by several authors (Wainman et al. (2001), Cazorla et al. (2012)) and tested by laboratory experiments in Cazorla and Brune (2010), is that NO_2 is lost via reactions on the sample chamber walls, and is catalyzed in the presence of higher relative humidities. This first field deployment was successful in providing a first test of atmospheric oxidation chemistry and testing the theory behind the MOPS. However, more laboratory testing of the MOPS chamber chemistry was needed to substantiate its results.

2.1.2 MOPSv2.0

A common characteristic of both indoor and outdoor environmental chambers is that they can exhibit chemical processes unlike the atmosphere because of surfaces in the chamber. Chamber walls can remove gas-phase species as well as act as a surface onto which particles can deposit (Cocker et al., 2001). Although it is unclear whether wall effects played a dynamic role in the MOPSv1.0 behavior, much effort has been put into re-designing a second version of the Penn State MOPS, with a great deal of development concentrated on limiting the amount of time that sampled air is in contact with surfaces in the chamber.

A new MOPSv2.0 has been designed and two were built and deployed in 2013 and tested in two areas. Preliminary chambers were tested on the roof of Penn State University's Walker building. Two MOPSv2.0s were then deployed on the roof of University of Houston's 70m Moody Tower North and in Smith Point, TX during NASA's 2013 DISCOVER-AQ Texas field campaign. It is hypothesized that the developments

made to the second version of the Measurement of Ozone Production Sensor provide a more qualitative $P(O_3)$ measurement than the MOPSv1.0. In particular, this more robust, automated instrument is improved in several ways over the previous MOPSv1.0, including instrument design, measurement technique, and flow through the chambers. The MOPSv2.0 was designed with future goals to:

- provide a first step in determining ozone point sources and locations to which ozone is being advected
- be implemented into air quality networks to validate air chemistry models and pollutant regulatory strategies, and
- provide pertinent information as to when and where ozone production is NO_x-limited or VOC-limited.

The air flow through the chambers is critical. Air turbulence and convection can create interactions with air molecules and the chamber walls. Therefore, by controlling the airflow and the stability of the air in the chambers, it may be possible to reduce turbulent, convective eddies and thus wall interactions with the air sampled at the output of the MOPS chambers. The following technical section outlines a new MOPS structure design, and details developments made to control the airflow within the MOPS chambers.

2.2 Development of the MOPS Chamber and Flow Regime

The MOPSv2.0 chamber design is intended minimize potential wall effects and convective mixing. In order to maximize the exposure time, τ, airflow must either

be slowed down, or the MOPSv2.0 volume must be increased. Re-inventions to the MOPSv1.0 chamber design include developments in the shape, size, flow rates, and air stability and turbulence inside of the chambers.

2.2.1 Technical Description of MOPS Chamber

As in Cazorla and Brune (2010), both sample and reference chambers of the MOPSv2.0 are identical in size and shape. Instead of a cylindrical shape in the original MOPS, these new chambers are designed to mechanically force air from the entrance towards the exit of the chamber, accelerating exiting air into an "exit cone" out of which O3 + NO_2 will be measured by the ozone monitor. The new chamber frames are trapezoidal in shape with a larger entrance than exit area. Similar to Cazorla and Brune (2010), Teflon film (FEP, 5mm thick) is wrapped around the chamber frame and serves as the chamber walls. The total flow through each chamber is 23 liters per minute (LPM),significantly faster than the original MOPSv1.0. As a consequence of higher flow rates, the total volume of a MOPSv2.0 chamber is increased from the pre-existing 11 liters (L) to 26.9L in order to maintain a sufficient exposure time for the chemical reactions to produce a measurable amount of ozone in the sample chamber. The MOPSv2.0 has a smaller chamber surface area to volume ratio, which can be advantageous when minimizing wall effects because less air can come in contact with the walls (Cocker et al., 2001). Figure 2.2 provides a schematic and outlines the flow of the new MOPSv2.0 chambers.

2.2.2 Technical Description of Chamber Flow

The chambers and flow regimes are designed with the intent to preserve laminar flow. Air is pulled into and through the chambers with a rotary pump. The chamber is designed to produce an airflow like a sheath flow with higher bypass flows on the tops and sides of the chambers, and lower sampling flows through the middle and exit cone. An outer, sheath flow is pulled by a bypass pump at 20LPM, while an inner, sampling flow through the exit cone is set to 3.2LPM. To eliminate any possible pressure gradients along the exit face of the chamber, the sampling to bypass flow ratio is equal to the ratio of the exit cone surface area to the bypass exit plane area.

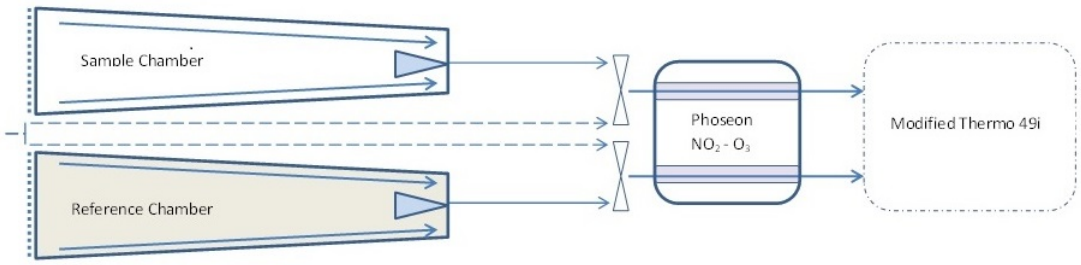

Fig. 2.2. Schematic of MOPSv2.0. Air is sampled continuously through the open-faced sample and reference chambers. A rotary pump pulls a total of 23LPM: the bypass flow along the sides, tops, and bottoms of the chambers pulls 20LPM, while the exit cone flows pull sampling air at 3LPM. Bypass airflow is exhausted, while the exit cone airflow enters the NO_2-to-O_3 converter.

The flow in the chambers is intended to be much like flow through a pipe. A Reynolds number (Re) of 783 was calculated for the flow in the chamber, given the above flow rates, an average area of $0.026m^2$, and a kinematic viscosity coefficient of

$1.52E^{-5} m^2 s^{-1}$. Because the critical Reynolds number, Re_{crit}, that separates laminar from turbulent flows is 2300, the flow inside of the chambers is laminar (Spurk and Aksel, 2008).

This flow regime is intended to reduce the sampling of air that has interacted with the walls, which are capable of both removing or adding unwanted chemicals to the air. Air flowing near the walls of the chamber is accelerated along the walls and into the bypass flow where it is exhausted. Meanwhile, air flowing near the center of the chamber stays in the center, is accelerated into the exit cone, and is sampled by the ozone monitor.

2.2.3 Addition of Laminar Mesh Screening and Heating Elements

In order to preserve laminar flow through the chambers and suppress convective eddies, coated laminar mesh screens have been added to the chambers. The control of the velocity distribution of a fluid flow has long since been recognized as a fundamental problem in fluid mechanics, as reviewed by Laws and Livesey (1978). However, one way to resolve time-mean velocity non-uniformities, increase resistance in entering flow, and control downstream flow is through wire gauze screens. The following technical work highlights the use of these screens as well as a "heating grid" to suppress convection and increase stability in the chambers.

Air enters the MOPS chambers through a lattice face, which is open to ambient air. This lattice (Teflon FEP, 10mm thick) is perforated with holes 0.95cm diameter, yielding approximately 8% of open area on the lattice face. This technique yields a chamber residence time closer to a theoretical "plug flow" residence time of air molecules

in the chamber, by reducing the fast jetting of air into the body of the chamber that was evident in the MOPSv1.0 chambers. Air entered the MOPSv1.0 entrance face of a 120cm diameter cylindrical chamber through an inlet (1.27cm diameter) that reduces the open area to 0.5%. Because the total MOPSv1.0 flow rate of 1LPM was pulled through an open area of 0.5%, this design increased the fast jetting of air into the MOPS chamber and turbulent mixing, and decreased the residence time in the chambers.

To control the downstream air velocity distribution, laminar wire mesh screen (Stainless Steel, 0.03cm diameter wire, 41% open area) is added behind the lattice face in MOPSv2.0. This mesh is coated with Silconert, an inert chemical coating that greatly reduces any potential chemical reactions of air with oxygenated species on the surface of the mesh (SilcoTek, 2014).

Stability of air entering the chambers is increased with the addition of a heating "grid" downstream of the lattice and laminar mesh. The heating grid creates a thermal increase from the bottom to the top, which enhances vertical stability and suppresses convection. This heating component is comprised of three sections of evenly-spaced wire (32 BNC). Each wire portion of the heating grid has decreasing resistance from top to bottom so that the uppermost portion is heated more than the lowermost portion and creates a slight positive temperature gradient from the bottom to the top of the entrance face. A few degrees is more than sufficient to create and maintain stability in the air as it flows through the chambers.

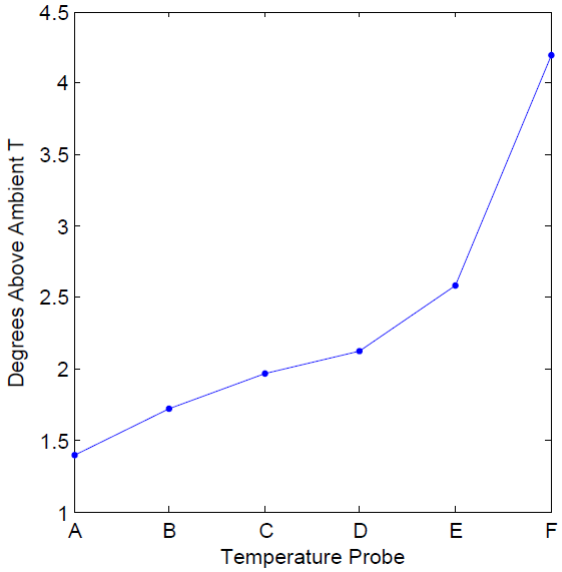

Fig. 2.3. Vertical temperature distribution in the MOPSv2.0 chamber measured with a six-thermistor temperature probe. Temperatures were measured every 2.5cm from the top to the bottom of the chamber. Thermistor A corresponds to the temperature at the lowermost portion of the chamber, while Thermistor F corresponds to the uppermost temperature.

Laboratory flow visualizations have shown that even a temperature gradient of less than 0.5 degrees C can cause convective mixing of air inside of the chamber. By heating the air approximately four degrees above ambient temperature at the top of the entrance face and one degree above ambient temperature at the bottom of the entrance face, convective mixing in the chamber is expected to be highly suppressed. To measure the vertical temperature distribution in the MOPSv2.0 chamber, a six-thermistor temperature probe was inserted into the chamber approximately three inches away from the heating grid. The vertical temperature distribution for the MOPSv2.0 chamber is shown in Figure 2.3.

Behind the heating grid lies an additional Silconert-coated laminar mesh (Stainless Steel, 40um filter size, 5mm diameter wire) screen to decrease laminar flow disturbances by dissolving any convective eddies entering the chamber face.

After air in the center of the chamber is pulled to the back of the chamber as described above, it enters the exit cone (3.5cm diameter, Teflon FEP), which protrudes through another laminar mesh bypass screen (Stainless, 40um filter size, 5mm wire diameter) acting to provide even resistance to the faster bypass flow. The bypass air is pulled through the exit screen and exhausted, while the ozone monitor samples the air entering the exit cone. Additional laminar mesh exit screens (Stainless Steel, 0.03cm wire diameter, 41% open area) are placed behind the exit screen in the rear cap of the chamber to uniformly pull air at the exit plane towards the bypass pump, where it is exhausted.

2.3 Development of the MOPS P(O_3) Measurement Technique

Several developments have been made to the MOPS chamber design and flow regime to make the MOPSv2.0 more robust and sophisticated. These include fully automating the MOPS sampling process, installing a highly efficient ultraviolet (UV) light-emitting diode (LED) NO_2-to-O_3 converter, and implementing DewLines® in the modified ozone analyzer to deter water vapor interference in the O_3 measurement. All of these improvements help to make a more qualitative and robust P(O3) measurement.

2.3.1 Full Automation of the MOPSv2.0 Measurement

The first improvement made to the MOPS P(O_3) measurement itself includes full automation of the measurement process. For the first time, the MOPSv2.0 can run continuously on its own without human operation. A LabView interface coupled with National Instruments data acquisition was designed to control the MOPSv2.0 measurement and collect the data. This allows the user to set various parameters in the interface, as well as to monitor sensor output.

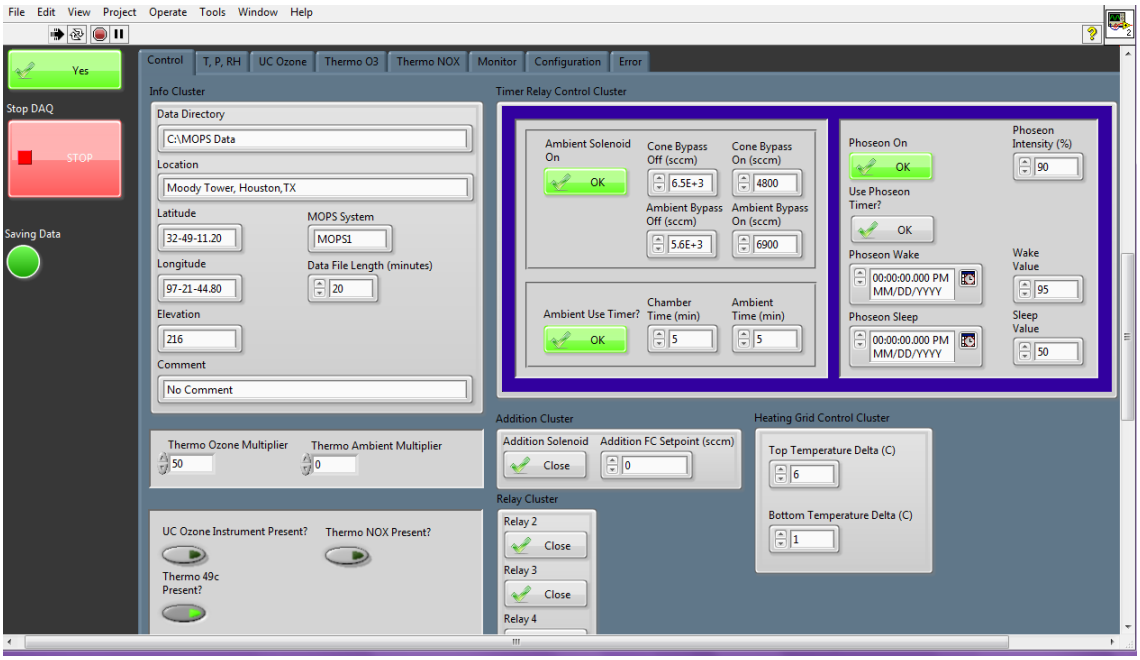

Fig. 2.4. MOPSv2.0 system control interface in LabView

In total, over 50 parameters are read and stored in the data files every second. With such extensive monitoring of the MOPSv2.0 system, diagnosing and repairing

software, instrument, and data acquisition problems is faster and simpler than the MOPSv1.0. A schematic of the MOPSv2.0 Labview Control system interface is seen in Figure 2.4.

2.3.2 Phoseon® Ultraviolet Light-Emitting Diode Conversion Cells

A more efficient NO_2-to-O_3 converter has been implemented in the MOPSv2.0. Without an efficient conversion system, resulting ozone production rates can be biased. As the reference chamber ozone is mostly partitioned towards NO_2, the modified ozone analyzer will only read ozone that has been produced in the transparent sample chamber, resulting in a false ozone production rate.

The MOPSv2.0 converter is composed of two parts: a photolytic cell box and a UV LED lamp. This LED produces UV radiation (max irradiance = 2W cm^{-2}) at a peak wavelength of 395nm (Phoseon, 2012). In the photolytic cell, two Teflon end pieces encapsulate a pair of 38mm OD quartz tubes. The LED is mounted on top of the cell, while the other three sides of the cell are mirrored to reflect and expose the same amount of radiation to each quartz tube. The residence time of air inside of the photolytic cells is 37 seconds, and the intensity of the Phoseon LED is user-controlled via the LabView interface. Converter unit efficiencies are presented in the following chapter.

2.3.3 DewLine® Implementation

In addition to a fully automated measurement and a highly-efficient conversion unit, DewLines® were implemented in the modified Thermo 49i ozone analyzer for the MOPSv2.0 system. As in Cazorla and Brune (2010), the Thermo 49i ozone analyzer is

adapted to measure ozone from both the sample and reference chambers by removing the manganese oxide ozone scrubber that would otherwise be present in the reference sampling line. The sample and reference lines are then connected to the Thermo 49i UV absorption cells where the Beer-Lambert Law is used to calculate the concentration of ozone within the cells.

Wilson and Birks (2006) found that most commercial UV absorption analyzers, including Thermo manufactured analyzers have a water vapor interference that ranges from tens to hundreds of parts per billion by volume (ppbv). This water vapor interference is thought to stem from humidity effects on the transmission of uncollimated UV light through the detection cells. It was found that the insertion of a Nafion membrane tube just before the absorption cells decreased the interference to 2 ppbv (Wilson and Birks, 2006). Although the ozone scrubber acts as the main reservoir for adding or removing water from the detection cells, the DewLines have the potential to reduce this humidity interference between the two cells, thereby minimizing any differences between the sample and reference sampling lines. While the positive effects of the DewLines on the MOPS system have yet to be well understood, preliminary testing of these Nafion insertions are thought to have a positive effect in eliminating any water vapor interferences in the MOPS modified ozone analyzer.

Chapter 3

Experimental Methods and Diagnostics

3.1 Characterization of MOPSv2.0

Several factors must be known in order to obtain a qualitative $P(O_3)$ measurement: the residence time of air in the MOPSv2.0 chamber, the differences in the sum of O_3 and NO_2 between the two chambers, and any additional photochemistry in the chambers that may affect and bias the ozone production rate. The residence time and potential biasing photochemistry are both affected by the characteristics of the flow in the chamber. These key factors are examined below.

3.1.1 Chamber Heating Grid Stability Enhancement

The MOPSv2.0 heating grid creates a stable layer throughout the chamber by developing a positive temperature gradient from the bottom to the top of the chamber entrance face. This increased stability should suppress convective eddies in the MOPSv2.0 chamber flow and therefore wall interactions with sampled air. Although air in the MOPSv2.0 chambers is naturally stabilized by radiation during daylight hours as seen in Figure 3.1, shadowing within the chamber may cause a decrease in stability, especially during morning hours when ozone production is significant. If the chamber temperature profiles are not actively controlled, the sample and reference chambers may

have different profiles. This difference can lead to instability and chemical imbalances between the chambers.

Thermistors monitor the temperature gradients in the MOPSv2.0 chambers by measuring the temperature approximately 2.5 cm away from the top and bottom of the entrance and exit faces. Altogether, four temperatures are recorded in each chamber: sample (reference) inlet top/bottom and sample (reference) outlet top/bottom.

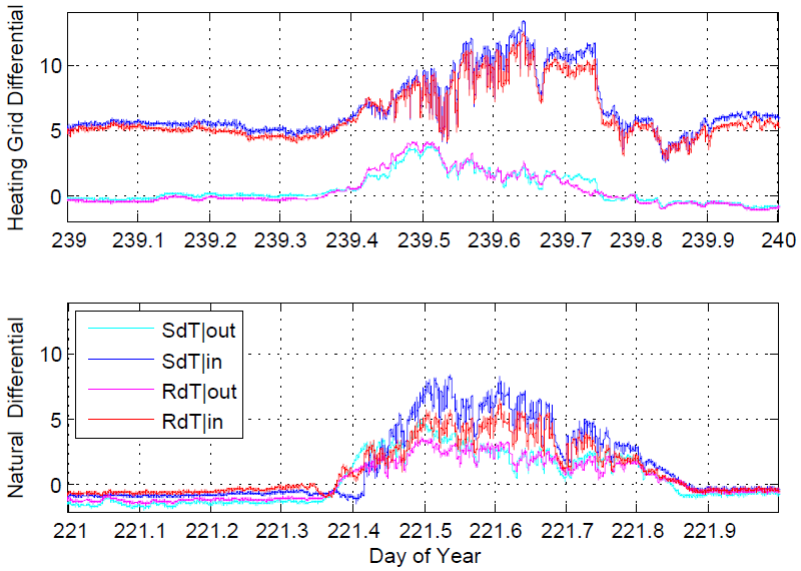

Fig. 3.1. Natural (bottom) and heating grid enhanced (top) temperature gradients in the MOPSv2.0 chamber. Temperature differentials for the sample and reference inlet and outlet (SdTin/out,RdTin/out) are computed by taking the thermistor measurement difference (top-bottom).

The heating grid controls and maintains a positive temperature gradient between the tops and bottoms of the chambers throughout the day, especially during crucial ozone production hours (Figure 3.1, top panel). More importantly, it retains fairly

consistent temperature gradients between the sample and reference chambers despite natural temperature fluctuations. Without the MOPSv2.0 heating grid (bottom panel), a distinct temperature gradient is not always present in the chamber from entrance to exit and inconsistent gradients develop throughout the day between the sample and reference chamber. With the heating grid enhancement, the average temperatures of the sample and reference chamber are within 2^{o}C of each other and are less than 5^{o}C different from the ambient temperature during the time of peak ozone production (Figure 3.2).

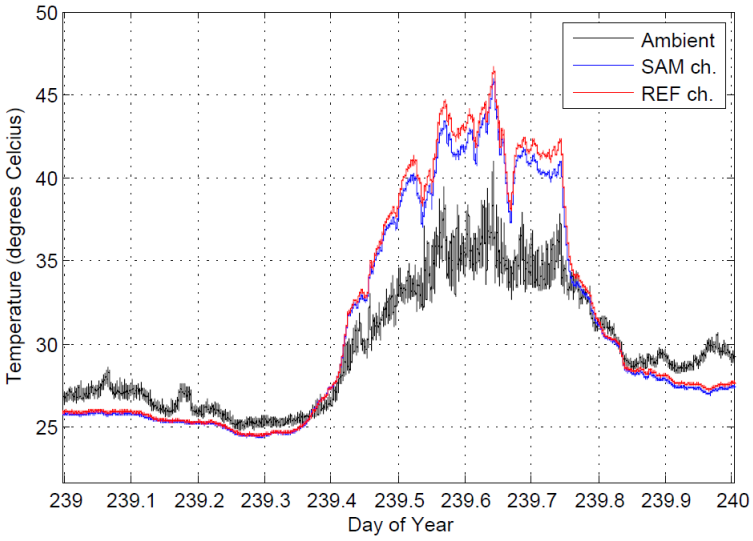

Fig. 3.2. Sample and reference chamber average temperatures in the MOPSv2.0 chambers including natural and heating grid enhanced temperature gradients.

3.1.2 Laboratory Testing of Flow Development

Extensive laboratory flow visualization testing was conducted to ensure that the sampling flow that enters the exit cone has limited interactions with the walls of the

chamber. This visualization was done by adding smoke to the chambers under heating-grid stabilization and examining its behavior in the chamber flow regime. Smoke was generated and cooled to ambient temperatures before adding it to the chamber through the lattice face and was monitored until its exit. Figure 3.3 depicts a smoke visualization experiment in the MOPSv2.0 chamber. The heating grid voltages and resistances were then determined by trial and error to best approximate "wall-less" chamber sampling flow with fairly straight streamlines of smoke and little obvious rotation.

Fig. 3.3. Image of smoke behavior in the MOPSv2.0 chamber

In general, the MOPSv2.0 flow regime allows sampled air to enter the chamber face without fast jetting of air and accelerate into the exit cone and along the surfaces of the chamber as expected. With the addition of the heating grid, air near the center of the chamber stayed in the center, and uniformly progressed to the exit of the chamber with very little convection. Any smaller, convective eddies near the walls of the chamber were

caught in the bypass flow and exhausted along the walls at the chamber's exit. Without the addition of the heating grid, convection dominates the top-bottom movement of airflow in the chambers as it moves non-uniformly to the exit face of the chamber.

3.1.3 MOPSv2.0 Chamber Exposure Time

Laboratory smoke visualization tests approximate the flow behavior in the chamber. However, a better approximation of the flow regime is found with ozone pulse tests, in which a short "pulse" of ozone is created at the entrance of the chamber using a mercury lamp and monitored at the exit. These tests assess the exposure time of air molecules in the MOPS chambers, the effectiveness of the sheath flow regime, and the increased chamber air stability with the inclusion of the heating grid.

The residence time of molecules inside the MOPSv2.0 chamber linearly affects the calculation of the hourly ozone production rate as seen earlier in Equation 2.1. For the sample chamber, the residence time is roughly equivalent to the amount of time that air in the chamber is exposed to photolysis. The theoretical residence time is calculated to be 72s, or 1.2 minutes, for a total flow rate of 23LPM and volume of 26.9L. This theoretical residence time describes a perfect plug flow, where every molecule spends exactly the same amount of time in the chamber.

For the MOPSv1.0, the theoretical residence time was approximately 450s or 7.5 minutes, while the actual residence time was 348s or 5.8 minutes. The difference of 102s is thought to stem from the fast jetting of air into the chambers and associated turbulent mixing. The normalized mean ozone distribution for MOPSv1.0 exhibits a long, slow

decay, or tail, which is a signature of turbulence and uneven mixing. This mixing can result in increased chamber wall interactions (Cazorla and Brune, 2010).

The residence time for the MOPSv2.0 was determined by adding a 20 second pulse to the entrance of the MOPS chamber, and measuring the ozone at the exit. The total mean residence time is calculated by Equation 3.1

$$\tau = \frac{\sum_{t=0}^{dt} [O_3(t)t]}{\sum_{t=0}^{dt} O_3(t)} \tag{3.1}$$

where O_3 represents the normalized ozone from 0 to 1. The mean ozone pulse distributions for both the MOPSv2.0 chamber sampling and bypass flows are similar, indicating that the flows patterns are the same between the sampling flow at the output and the flow near the walls that is exhausted. The associated residence time of the bypass flow near the walls was calculated to be 100s or 1.67 minutes, while the sampling flow residence time is 114s or 1.9 minutes (Figure 3.4). Because the bypass and exit cone flows are operated by mass flow controllers, the chamber residence time is accurate to within 10% with wind effects taken into account. The faster bypass flow exhausts the ozone pulse, leading to a shorter residence time for air molecules nearest the chamber walls while sampling air in the center of the chamber, which has limited contact with the chamber walls, has a longer residence time. These ozone pulse tests verify that the flow within the MOPSv2.0 chambers resembles a sheath flow regime, which decreases the possibility of sampling being affected by air wall interactions. In addition, the tail

of the ozone distribution is much shorter, which indicates a decreased amount of uneven and turbulent mixing.

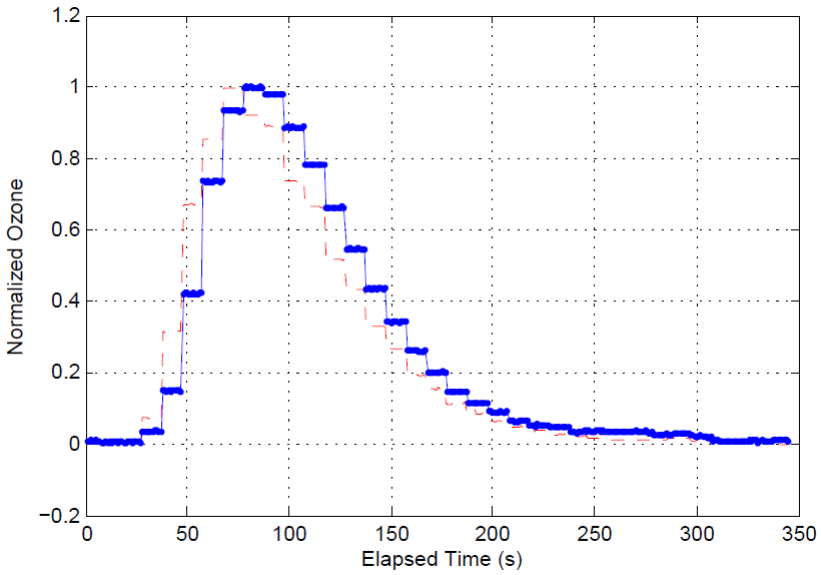

Fig. 3.4. Normalized ozone distribution for the bypass (red dashed) and exit cone (blue solid). The residence time in the chambers is calculated using Equation 3.1. In this case, the exit cone flow residence time was calculated to be 114s or 1.9 min, while the bypass residence time was 100s or 1.67min.

3.1.4 Measurement of Photolysis Frequencies

The ability of the MOPSv2.0 sample chamber to simulate the ambient ozone photochemistry and the reference chamber to eliminate it must be verified (Cazorla and Brune, 2010). Photolysis frequencies of the sample chamber for different thicknesses of Ultem films (0.003", 0.010") were examined for the MOPSv2.0 chamber. These measurements were made on a clear, sunny day (28 October 2013) on the roof of University

of Houston's Moody Tower North by B. Lefer using a Scanning Actinic Flux Spectroradiometer (SAFS) described by Shetter and Müller (1999) and Shetter et al. (2003).

Calculated values for the photolysis frequencies of HONO, O_3, and NO_2 in both the clear, sample chamber as well as 0.003" and 0.010" UV-coated reference chambers are given in Table 3.1. Measured SAFS JO_3, JHONO, and JNO_2 photolysis frequencies for the sample chamber are within 3% of the measured ambient values. The SAFS measurements for the thin Ultem film yielded photolysis frequencies of JO_3, JHONO, and JNO_2 that dropped to less than 2% of ambient values. Photolysis rates dropped to less than 1% of ambient values when measuring through the thick Ultem film.

As in Cazorla and Brune (2010), these measurements show that radical formation is suppressed in the MOPS reference chamber. Photolysis leading to radical production, including HONO and O_3 photolysis, is suppressed to less than 2% with both thicknesses of Ultem film. The thin (0.003") Ultem film adds value to the MOPSv2.0 measurement in that it has the potential to help minimize temperature differences between the sample and reference chambers without compromising UV transmittance effects. These photolysis frequencies will be used to characterize the MOPSv2.0 measurement with a simple photochemical box model.

	JNO_2 (s^{-1})	**JO_3 (s^{-1})**	**JHONO (s^{-1})**
Ambient	5.13E-03	9.75E-06	1.11E-03
Clear Teflon FEP (0.005")	5.08E-03	9.54E-06	1.09E-03
Ultem (0.003")	3.68E-04	3.16E-08	1.70E-06
Ultem (0.01")	5.24E-05	9.05E-09	2.01E-07

Table 3.1. Photolysis frequencies of JO3, JHONO, and JNO2 measured by the SAFS (B. Lefer) on a clear, sunny day in Houston, TX.

3.2 Photochemical Box Model Characterization of MOPSv2.0

The photochemical box model was used to examine differences between ozone chemistry in the MOPSv2.0 and the atmosphere. With this model, it is possible to characterize the MOPSv2.0 given ambient and Phoseon photolysis frequencies. The model is used to simulate the sample and reference chamber, the Phoseon®converter unit and atmospheric conditions. It contains rate reactions that include inorganic ozone photochemistry, reactions with OH and VOCs, and simplified organic radical (R) chemistry – particularly reactions of RO_2, HO_2, NO_2 and NO.

Sample and reference chamber model calculations are run in MatLab for a total of 200s with a time step of 0.008s, using measured sample and reference chamber photolysis frequencies given in Table 3.1. To simulate the Phoseon® converter unit, a separate model with different parameters is used. For all converter unit model calculations, the

model was run for a total of 38s with a time step of 0.008s and with a calculated NO_2 photolysis frequency of $0.23s^{-1}$.

3.2.1 Phoseon® Converter Unit Efficiency

Conversion efficiencies and corresponding NO_2 values are measured in the laboratory. Measurements are performed by flowing NO_2-containing air through the cells and monitoring the NO_2 output for varied NO_2 mixing ratios as the LEDs are turned on at 100% (Table 3.2). The measured conversion efficiencies were compared to those calculated with the photochemical box model, with the same NO_2 mixing ratios. For most cases, the control and measured conversion efficiencies compare quite well (R^2=0.95, N = 3), and for typical environmental levels of NO_2, the conversion efficiency is greater than 88% (Table 3.2).

Previous MOPSv1.0 NO_2 conversion efficiencies are displayed in Table 3.3 (Cazorla and Brune, 2010). The MOPSv2.0 Phoseon converter is an improvement over the MOPSv1.0 converter in that its efficiency is consistently higher at increasing nitrogen dioxide mixing ratios. For example, typical high NO_x conditions seen in Houston, TX ranged from 60-80 ppbv NO_2. The MOPSv2.0 conversion efficiency for this range of nitrogen dioxide is greater than 80%, whereas for MOPSv1.0, the conversion is approximated to be 66%. To estimate how this difference in efficiencies can affect the MOPS ozone production measurement, the photochemical model case was run for the following conditions: NO_2 = 75 ppbv, O3 = 10 ppbv, and NO = 0 ppbv. Assuming a change of ozone between the two chambers of 1 ppbv, a decrease in efficiency from 82% to 66% would result in a 6% decrease in the final measured production rate. Therefore,

MOPSv2.0's increased efficiencies of NO_2 conversion can result in a more accurate and quantitative P(O3) measurement.

NO_2 (ppbv)	**Sample (%)**	**Reference (%)**	**Average (%)**	**Model (%)**
5	94.8	98.3	96.6	95.9
20	88.2	89.0	88.6	92.2
40	86.9	89.3	88.1	88.0
60	83.6	83.6	83.6	84.5
80	82.4	82.4	82.4	81.4
110	78.1	78.5	78.3	77.5

Table 3.2. Measured converter efficiency for sample and reference photodiodes and comparison to model-calculated conversion efficiencies.

NO_2 (ppbv)	%Conversion
17	88
25	83
45	77
75	66
125	58

Table 3.3. MOPSv1.0 NO_2 converter efficiencies (Cazorla and Brune, 2010).

3.2.2 Converter Unit Characterization

The photochemical model is used to characterize the Phoseon® NO_2-to-O_3 converter. To ensure that the converter cell residence time is sufficient to allow for NO_x PSS to reach equilibrium, the NO_x PSS relaxation time is calculated. The total calculated residence time in the photodiodes is 37 seconds. Model results indicate that the time it takes for NO_x to reach steady state is approximately 20s, which is well within the residence time of air in the photodiodes. Addition of the converter unit reduces the difference between the two chambers to less than 0.2 ppbv hr^{-1}.

As seen in Table 3.1, the sample chamber is transparent to actinic radiation, and the reference chamber blocks all radiation of wavelengths less than 400nm. With this UV-blocking film, the NO_x PSS in the reference chamber shifts in the direction of NO_2 while the NO_x PSS in the sample chamber shifts towards NO and may partition into NO_2. Tables 3.2 and 3.3 indicate that NO_2 conversion decreases with increasing NO_2. As NO_2 increases, so does its photolysis rate and thus the rate of the reaction between NO and O_3 also increases to stay in NO_x PSS. In addition, as the UV LED output can shift NO back to NO_2 via reactions with ozone, increases in ozone also decrease the NO_2 conversion. This decrease in NO_2-to-O_3 conversion can result in a potential bias in the ozone production rate.

Model characterization of this bias allows for possible corrections to account for the decreased efficiencies that occur at higher values of NO_2 and O_3. Calculated efficiencies for values of NO_2 and O_3 less than 30 ppbv are greater than 90% (Figure 3.5). However, these values of NO_2 and O_3 are conservative for urban areas such as Houston,

TX, where NO_2 and O_3 values during peak ozone production hours can be as high as 60 ppbv and 50 ppbv. This increase in NO_2 and O_3 decreases the converter efficiency to approximately 83%. To encompass all possible NO_2 + O_3 values typical of the 2013 Houston, TX measurement period, we consider relevant only NO_2 less than 60 ppbv and O_3 less than 90 ppbv. Conservatively, the lowest conversion efficiency that can result from these values adds a potential 15% negative bias (3 ppbv hr^{-1}) to the MOPSv2.0 measured ozone production rate.

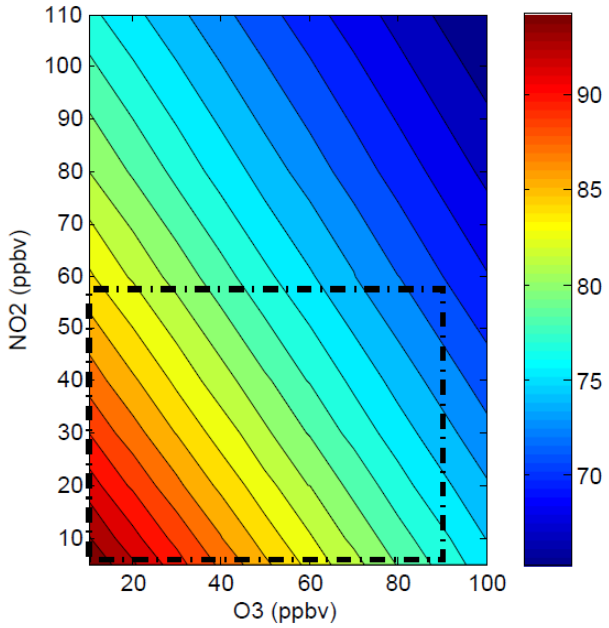

Fig. 3.5. Phoseon®conversion efficiency contours for various initial NO_2 (ppbv) and O_3 (ppbv) ratios. Typical combinations (dotted box) of NO_2 + O_3 exhibit a potential bias <= 15% (3 ppbv hr^{-1} difference) due to decreased conversion efficiency.

3.2.3 MOPSv2.0 Sensitivity to Photostationary State Differences

The differences in NO_x PSS between the sample and reference chamber and the effectiveness of the Phoseon® to balance these differences is salient for a quantitative MOPSv2.0 measurement. In some cases, the differences in NO_x PSS between the sample and reference chambers may be large. This difference calls for high Phoseon conversion efficiencies to correct for these imbalances before sampled air (O_3 + NO_2) is measured by the ozone analyzer.

A simple sensitivity analysis was conducted using the photochemical box model to examine the sensitivity of the MOPSv2.0 converter unit to realistic early morning, mid-morning, and afternoon O_3 and NO_x ratios. Typical amounts of NO_x and O_3 were extracted from SHARP 2009 data in Houston, TX. In each case, the model was first run for sample and reference chamber photolysis conditions using measured photolysis frequencies (Table 3.1). The NO, NO_2 and O_3 output was then used to initiate a second model run using converter unit photolysis rates. The model was run a final time with a simulated 1 ppbv of ozone production in the sample chamber and the resulting ozone differential ($\triangle$ O_3) between the two chambers is calculated (Table 3.4). If the conversion efficiency is 100 %, the 1 ppbv ozone addition in the sample chamber should result in a 1 ppbv increase in $\triangle O_3$f between the sample and reference chambers.

Case Study	**NOi (ppbv)**	**NO_2i (ppbv)**	**O3i (ppbv)**	**$\triangle$ O_3f**	**(%)Error**
Mid-afternoon: Low NOx, high O_3	0.2	2	75	1	0
Early morning: Low NOx, residual O_3	1	5	30	0.99	1
Afternoon: Low NOx, average O_3	0.2	8	30	0.98	2
Late afternoon: Low NOx, low O_3	2	10	10	0.97	3
Afternoon rush hour: Low O_3	2	10	25	0.97	3
Early morning: Average NOx, low O_3	2	30	10	0.93	7
Mid-morning: High NOx, residual O_3	20	40	20	0.88	12
Early morning: High NO_2, low NO, O_3	0	60	5	0.88	12
Early morning: High NO_2, low O_3	10	60	10	0.86	14
Early morning: High NOx, residual O_3	10	60	30	0.85	15

Table 3.4. MOPSv2.0 sensitivity to various NO_x-O_3 ratio cases.

Several early morning, mid-morning, and afternoon cases representative of the Houston, TX summer are given in Table 3.4. The greatest differences between NO and NO_2 directly affect the NO_2 conversion efficiency as the sample chamber and reference chambers will have the greatest difference in NO_x PSS. As discussed above, if O_3 amounts are relatively high, the conversion efficiency is further decreased. For morning cases with NO greater than 10 ppbv and NO_2 greater than 40 ppbv, the decreased conversion efficiency creates a bias in the MOPSv2.0 P(O_3) measurement between 12% and

15%, respectively. As NO_x decreases throughout mid-late morning and ozone begins to increase, this bias decreases to less than 10%. Later in the day, ozone has reached its peak diurnal concentration while NO_x may increase due to Houston rush-hour traffic. For this time, the conversion efficiency bias in the ozone production rate is less than 5%. This analysis indicates that the maximum potential bias for typical Houston NO, NO_2 and O_3 scenaries is less than 20%, which occurs before $P(O_3)$ has reached its peak production rate.

3.2.4 Characterization of Nitrous Acid in MOPSv2.0 Chambers

Nitrous acid (HONO) is an important radical precursor and can affect the HO_x ($OH + HO_2$) budget as 20% of the daytime HO_x OH source can come from HONO photolysis (Czader et al. (2012), Ren et al. (2013)). Specifically, HONO photolysis is an important OH radical source both in the atmosphere and in the MOPSv2.0 chambers (Rohrer et al., 2005). The efficacy of the MOPSv2.0 flow regime in deterring wall interactions can be tested by comparing ambient and chamber HONO mixing ratios. Furthermore, HONO measurements done to test MOPSv2.0 may apply to other environmental chamber research and ozone chemistry.

The gas-phase reaction of OH and NO is one known pathway for HONO production (Reaction 3.22). Another slower mechanism is the heterogeneous dark formation on surfaces from nitrogen dioxide (Reaction 3.24). While the exact mechanism has not been identified, HONO production is thought to be catalyzed on surfaces from the photolysis of adsorbed NO_2 (Czader et al. (2012), Rohrer et al. (2005)). Although HONO production in environmental chambers is still unclear, laboratory results suggest that

it has a strong dependence on irradiation, temperature, and relative humidity (Rohrer et al., 2005).

$$OH + NO \longrightarrow HONO \quad \{3.22\}$$

$$Y(HONO) + h\nu \longrightarrow HONO \quad \{3.23\}$$

$$2\,NO_2 + H_2O \longrightarrow HONO + HNO_3 \quad \{3.24\}$$

Differences in HONO between the MOPSv2.0 chambers can result in a HO_x imbalance and ultimately, a false ozone production signal. Because of the suppression of HONO photolysis in the reference chamber, it is possible for the sample chamber to exhibit increased ozone because of sunlight-induced HONO production, leading to a positive bias in $P(O_3)$ from this additional OH source. HONO should be formed on the MOPSv2.0 chamber walls, as on the walls of other Teflon FEP chambers in Rohrer et al. (2005), but the sampled air in the MOPSv2.0 should contain much less HONO because the flow appears to be quite laminar and stable. However, the sampled air at the output of the MOPSv2.0 chambers must pass through the perforated Teflon sheet and two Silconert-coated stainless steel screens that are necessary to create stable flow. These surfaces may be a source of HONO when they are sunlit.

To begin to understand MOPSv2.0 chamber HONO production, nitrous acid was measured in both the sample and reference chambers in Houston, TX with a LOPAP3 (LOng Path Absorption Photometer). HONO in the MOPSv2.0 sampling air is measured in the gas phase by wet chemical sampling and photometric detection. Because HONO

production depends on sunlight, the HONO production on MOPSv2.0 surfaces were studied in an Ultem-covered reference chamber in which the walls were shielded from actinic radiation.

HONO is first measured in ambient, sample, and reference chamber conditions under full sun. Next, the effects of the heating grid on the sampled HONO mixing ratio were measured for heat 'ON' and heat 'OFF' conditions. The contribution of the chamber surfaces to HONO production within an Ultem-covered chamber was then examined by removing the Teflon lattice face and laminar mesh screen in front of the MOPSv2.0 heating grid.

The photochemical model is run to simulate the chemistry in the MOPSv2.0 operational mode. That is, the model is first run for sample and reference chamber conditions, and then the output of the chamber models is inputted into the converter unit model. Typical mid-morning initial conditions as seen on 28 October 2013 in Houston, TX are held constant in each chamber run and are chosen to be 30 ppbv O_3, 6 ppbv of VOCs (where VOCs are reactants that creates RO_2), 5 ppbv NO_2, and 1 ppbv NO. Finally, HONO-induced $P(O_3)$ is calculated from the final ozone for the sample and reference chamber and is compared to $P(O_3)$ calculated from ambient HONO mixing ratios in order to examine any positive bias that HONO production within the chambers adds to the MOPSv2.0 measurement.

Model results for HONO measurements taken on 28 October 2013 are shown in Table 3.5. For ambient HONO mixing ratios of 0.15 ppbv, the MOPSv2.0 ozone production rate is modeled to be less than 2 ppbv hr^{-1}. For full sun conditions, the measured HONO in the sample and reference chambers was 1.6 ppbv and 0.6 ppbv. This

difference in HONO between the two chambers has the potential to add an estimated 13 ppbv hr^{-1} bias to the $P(O_3)$ measurement. When the heating grid is turned off, the HONO measured through the sample and reference chambers is 1.7 ppbv and 0.7 ppbv, which creates an increased potential positive bias of up to 15 ppbv hr^{-1}. As the chambers are covered with Ultem film which suppresses HONO photolysis, the HONO in the sample and reference chambers were approximately the same with mixing ratios of 0.5 ppbv. Removing the Teflon lattice face and one Silconert-coated stainless steel screen slightly decreased the HONO mixing ratio in the chambers to 0.4 ppbv, yielding a positive bias of less than 5 ppbv hr^{-1}.

This bias may be dependent upon sunlight, relative humidity, and whether the ozone production is NO_x-sensitive or VOC-sensitive. The modeled $P(O_3)$ dependence on HONO is approximately linear, which suggests that the ozone production regime for this particular day was VOC-sensitive. A NO_x-sensitive regime would suggest that the ozone production rate is dependent upon the square root of the HO_x production (Seinfeld and Pandis, 2006).

With the heating grid increasing the stability within the chamber, there should be fewer wall interactions, and consequently, lower measured HONO mixing ratios if it is being produced on the walls of the chamber. With the MOPSv2.0 heating grid turned off, there was very little change in the HONO-induced $P(O_3)$ bias. This result is likely due to one of two possibilities: the chamber design is not as effective in minimizing wall effects as the flow visualization and ozone pulse tests suggest, or the measured HONO in the MOPSv2.0 chamber is produced through NO_2 photolysis on the entrance surfaces of the chamber before air is stabilized with the heating grid. Several surfaces are present

in the MOPSv2.0 chamber entrance including the Teflon FEP lattice face, two coated laminar mesh screens, and the MOPSv2.0 entrance face frame.

Condition	**Heat ON Y/N**	**HONO (ppbv)**		**P(O_3) (ppbv hr^{-1})**	**Bias (ppbv hr^{-1})**
Ambient	-	0.15		1.8	0
		SAM	**REF**		
Sun	Y	1.6	0.6	14.4	12.6
Sun	N	1.7	0.7	16.2	14.4
Ultem	Y	0.5	0.5	7.2	5.4
Ultem w/o Surfaces	Y	0.4	0.4	5.4	3.6

Table 3.5. MOPSv2.0 modeled P(O_3) from measured HONO within the sample and reference chambers. "Sun" cases reflect HONO measurements taken in full sun conditions, while "Ultem" cases represent HONO measurements taken when the chamber was covered with the Ultem (0.010") film. "Surfaces" removed include the MOPSv2.0 Teflon FEP lattice face and one laminar mesh screen.

Laboratory experiments show that the elimination of the MOPSv2.0 heating grid has a dramatic effect on the MOPSv2.0 chamber flow, and so the addition of the heating grid should greatly reduce chamber turbulence, wall interactions, and HONO production. Thus, it seems most likely that the photo-enhanced HONO production occurs on the entrance surfaces of the chamber. Table 3.5 also shows that, with the addition of the Ultem film and the blockage of NO_2 photolysis, the HONO mixing ratio is reduced by 70%. Thus, it may be possible to reduce HONO formation by shading the entrance films

and screens. Further HONO tests will be required to determine the exact location of HONO production in the MOPSv2.0 chambers.

With the assumption that the 28 October case is representative of typical HONO mixing ratios in the MOPSv2.0 chambers, the MOPSv2.0 $P(O_3)$ measurements could exhibit a positive bias of up to 15 ppbv hr^{-1} in high NO_x regimes. For days where ozone production was relatively low, we would expect the MOPSv2.0 to measure ozone production rates of at least 15 ppbv hr^{-1}, reflecting this bias. During these days, an ozone production rate of approximately 10-20 ppbv hr^{-1} is measured during the morning hours but this positive bias is not evident in the afternoon. One explanation for this result could be that photolysis from early morning NO_2 adsorbed on the entrance face of the MOPSv2.0 chamber produces added amounts of HONO in the chamber during the morning hours, but because of lower afternoon NO_2 mixing ratios, is not seen later in the day.

3.3 MOPSv2.0 Raw Data Processing

The procedure to determine the ozone production rate is based on the simple equation, Equation 2.1, but signal drifts occur due to variations in the ozone instrument and the chambers. The ozone differential between the sample and reference chamber is measured by a modified ozone analyzer at a sampling rate of 1 Hz and an averaging time of 10s. In an ideal situation, the only difference between the sample and reference photolytic cells is the excess NO_2 and resulting excess ozone produced in the sample chamber. However, various factors contribute to interferences in the ozone differential signal including possible minor differences between the two MOPSv2.0 chambers.

3.3.1 MOPSv2.0 Chamber and Ambient cycling

The MOPSv2.0 modified ozone analyzer is intended to be used in temperature and humidity controlled environments and measures ozone changes on the scale of several ppbv hr^{-1} over many hours. It has long been recognized that interferences arise in this measurement. Causes for oscillations in the ozone analyzer zero are still unknown, but are believed to be aggravated by inlet lines, filters, and most importantly, the modified ozone analyzer scrubber (US EPA, 1999). It was found that for most interferences, the effect on the ozone measurement under ambient conditions is minimal for typical ozone monitor operational modes (Kleindienst et al., 1993). Because the MOPSv2.0 differential measurement captures very small (<1 ppbv) changes in ozone between the sample and reference chambers, even the smallest ozone analyzer interferences can have a large impact on the MOPS $P(O_3)$ measurement. The removal of the MOPSv2.0 modified ozone analyzer scrubber, appropriate care to ensure inlet lines are consistent between both photometric cells, and addition of Dewlines® are all positive adjustments to the above mentioned interferences.

Commercial ozone monitors were not designed to be used the way they are in the MOPS and as a result can experience frequent zero drifts. This drifting can affect the ozone differential measurement and create false ozone production or destruction signals in the raw data. It is probably possible to reduce the effect of this zero drift by increasing the detection sensitivity and stabilizing the instrument temperatures, and this work will be part of the development of MOPSv3.0.

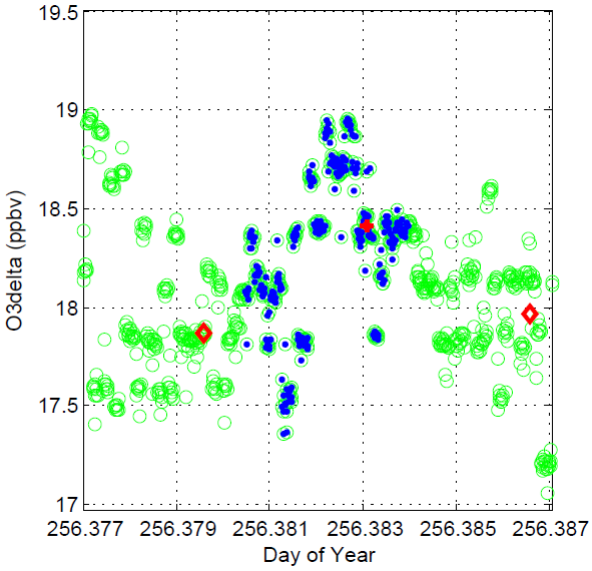

Fig. 3.6. The average of the median (red diamonds) raw ozone measurement from ambient air is subtracted from the median raw ozone measurement (red asterisk) from chamber air to find the ozone differential signal. Ambient cycling takes into account the drift in the Thermo 49i ozone analyzer signal.

The MOPSv2.0 ozone analyzer zero drift is accounted for by cycling the flow between chamber air and ambient air. As mentioned earlier, chamber sampling air is pulled at a flow rate of 3LPM from both chambers and measured by the ozone analyzer for a total of five minutes. Alternately, two "ambient" lines pull ambient air at the same flow rate for five minutes. Depicted in Figure 2.2, automated cycling between chamber and ambient air is identically controlled by three-way solenoids by the MOPSv2.0 LabView Control panel. Theoretically, both lines of ambient air will measure the same ozone amounts, thus acting as an automated zero for the ozone analyzer every five minutes.

To allow time for all of the air from the previous measurements to clear the chambers and to account for possible flow imbalances in the chambers during solenoid switches, the first 150 seconds of data points in raw measurement cycles are discarded. To objectively calculate the ozone differential, the median of the remaining points for both ambient and chamber cycles is found (Figure 3.6). The ozone differential is obtained by averaging the medians of the ambient cycles on either side of the chamber cycle, and then subtracting this from the chamber median signal. This method of computing the MOPS ozone differential results in a $P(O_3)$ measurement every 10 minutes.

3.3.2 MOPSv2.0 Chamber Zero Correction

In addition to the zero drift interferences, it is also necessary to account for differences between the MOPSv2.0 chambers. In theory, the MOPS chambers are identical, however minor differences in chamber shape, structural components, and build are inevitable. These differences between the MOPSv2.0 chambers affect the chamber chemistry and may stem from factors ranging from non-identical chamber components to slight temperature and relative humidity imbalances. Ideally, air composition and chemistry in the sample and reference chambers will be identical, with the exception that all radical chemistry will be eliminated in the reference chamber. However, the addition of the Ultem film inherently creates chemical differences between the sample and reference chamber.

After the ozone differential between the sample and reference chamber is found, the raw ozone production rate (ppbv hr^{-1}) is calculated by dividing the ozone differential

by the mean chamber residence time (Figure 3.7, second panel). Then, the raw production rate is corrected by applying a "chamber" zero, which aims to take into account the possible differences in the chamber chemistry as mentioned above.

A chamber "zero" is approximated by periodically removing the Ultem film from the reference chamber and calculating the net $P(O_3)$ between the two transparent chambers. This $P(O_3)$ zero is represented in Figure 3.7 (third panel, red circles), and acts as a baseline from which to subtract the MOPSv2.0 raw $P(O_3)$. The corrected $P(O_3)$ time series for Houston, TX is plotted against the raw measurement in the final panel for Figure 3.7.

As seen in Figure 3.7, the chamber zero technique corrects the raw measurement fairly well. However, it does not completely correct for the negative values seen in the measurement, which implies that there still exist unknown differences between the chambers that need to be resolved.

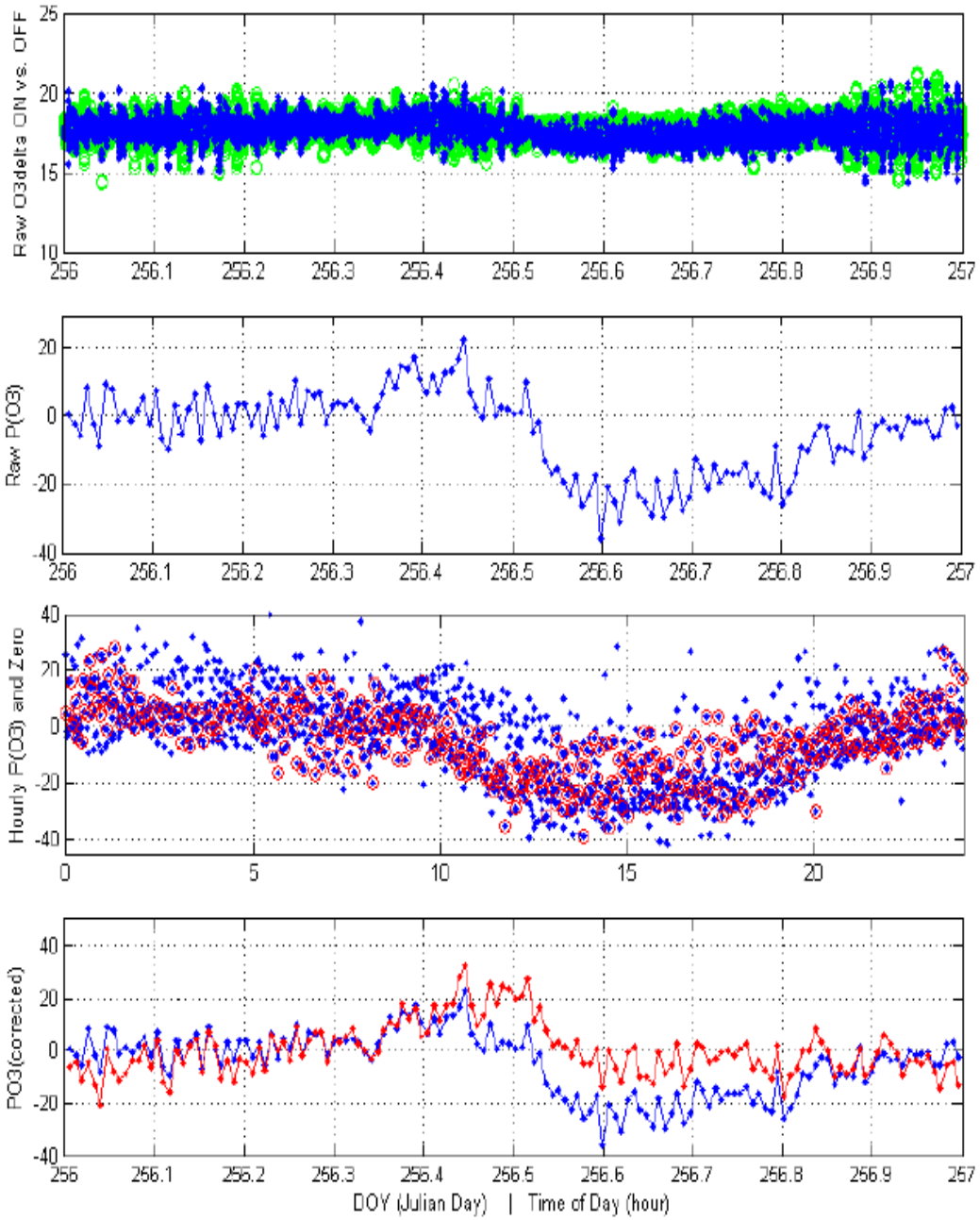

Fig. 3.7. Panel 1: MOPS ozone differential in chamber (blue) and ambient (green) cycles. Panel 2: Raw $P(O_3)$(ppbv hr^{-1}) without "chamber" correction. Panel 3: MOPS $P(O_3)$ (blue) and $P(O_3)$ zero (red) (ppbv hr^{-1}). Panel 4: MOPS raw (blue) and corrected (red) ozone production (ppbv hr^{-1}).

3.4 MOPSv2.0 $P(O_3)$ Sensitivity and Absolute Uncertainty

The MOPSv2.0 detection limit and sensitivity are obtained from the residence time of air molecules in the sample and reference chambers. The estimated limit of detection without the inclusion of the ozone analyzer zero drifting is 0.5 ppbv per five-minute cycle time, which corresponds to 6 ppbv hr^{-1}. However, due to frequent fluctuations in the ozone analyzer zero drift, this estimated limit of detection is low. This zero drifting can create an additional 10 ppbv hr^{-1} uncertainty in the limit of detection. Thus, the absolute limit of detection for the MOPSv2.0 instrument is estimated to be approximately 15 ppbv hr^{-1}. Conservative levels of ozone production in cleaner, more remote environments are less than or equal to 5 ppbv hr^{-1} (Cazorla and Brune, 2010). Production rates of highly polluted areas such as Houston, TX can exceed 50 ppbv hr^{-1}. Therefore, although the current MOPSv2.0 is not sufficient to accurately measure $P(O_3)$ in a relatively clean or remote atmosphere, it is more than adequate for urban environments that exhibit greater amounts of pollutants.

$$E_f = \sqrt{(\frac{\sigma_a}{\bar{a}})^2 + (\frac{\sigma_b}{\bar{b}})^2 + ...} \tag{3.2}$$

Statistically, the propagation of error is calculated to obtain an instrument's absolute error using Equation 3.2. The absolute $P(O_3)$ measurement error is primarily a function of the uncertainties in the ozone analyzer zero drift, residence time in the MOPSv2.0 chambers, and Phoseon® conversion efficiency. The largest errors associated with the residence time in the MOPSv2.0 chambers and converter unit are 10%, and 15% respectively. However, because the largest source of uncertainty stems directly

from the ozone analyzer drifting, the ozone differential, $\triangle O_3$, is used to calculate an absolute error in the $P(O_3)$ measurement. Thus, the first and only term in Equation 3.2 is $\frac{\sigma_{\triangle O_3}}{\triangle O_3}$. Instead of calculating a relative error, the absolute error is calculated by estimating the standard deviation of a set of data. The MOPSv2.0 dataset estimated standard deviation, $\sigma_{\triangle O_3}$, is approximately 1.7 ppbv over the five minute cycle time, which corresponds to a standard deviation in the MOPSv2.0 $P(O_3)$ measurement of 20 ppbv hr^{-1}.

The MOPSv2.0 $P(O_3)$ measurement includes various biases that add to the uncertainty in the MOPSv2.0 measurement such as HONO production within the MOPSv2.0 chambers, converter unit efficiency, reference and sample chamber photolysis frequencies, and losses of constituents on the walls of the chambers. HONO production inside of the MOPS chambers has the potential to add roughly 15 ppbv hr^{-1} to the MOPSv2.0 measurement, although more analysis is needed to verify when and where the production is taking place. The bias in the MOPSv2.0 PO_3 measurement due to converter unit efficiency is expected to be less than 15% for typical urban NO_x and O_3 mixing ratios. Losses of oxygenated species are expected to be minimal with the addition of the Silconert® mesh screens and flow regime, although rigorous testing of these losses is required.

Chapter 4

Results: DISCOVER-AQ Texas, Summer 2013

Two MOPSv2.0s, labeled MOPS1 and MOPS2, were built and deployed to Houston, TX for NASA's "Deriving Information on Surface conditions from COlumn and VErtically resolved observations Relevant to Air Quality" (DISCOVER-AQ) field campaign in August 2013. Preliminary MOPS1 and MOPS2 setup and measurements took place from early August to 1 September 2013, where both MOPSv2.0s were positioned in Houston, TX. The Houston measurement site was located 70m above the ground on the roof of University of Houston's Moody Tower North, an 18-story residence hall. This site can be influenced by petrochemical emissions from Houston's ship channel to the east and vehicle emissions from the Houston metropolitan region to the northwest.

From September to October 2013, MOPS1 was transported to the DISCOVER-AQ Smith Point, TX site located southeast of Houston's ship channel where it obtained $P(O_3)$ measurements on the roof of Penn State's NATIVE trailer 8m above the ground. At the same time, MOPS2 continued to gather $P(O_3)$ measurements at the Moody Tower site. Inter-comparisons between the two MOPSs were obtained from 1 to 28 October 2013 with MOPS1 and MOPS2 simultaneous measurements at Moody Tower. The MOPSv2.0 objective was to test the new MOPSv2.0 design and measurement techniques, to measure and compare ozone production rates both in Houston and in Smith Point, TX, to

characterize ozone advection and point sources of ozone, and to inter-compare MOPS1 and MOPS2 when they were both running at the same location.

In addition to real-time P(O_3) measurements, a full suite of meteorological variables and atmospheric species were measured on the Moody Tower roof by a University of Houston instrument suite and at Smith Point by an instrument suite located in Penn State's NATIVE trailer (Table 4.1). A map of the Smith Point, TX and Houston, TX measurement sites are shown in Figure 4.1.

Measurement	**Moody Towers: Houston, TX**	**Smith Point, TX**
Temperature	MOPSv2.0 thermistor	MOPSv2.0 thermistor
Relative Humidity	MOPSv2.0 RH sensor	MOPSv2.0 RH sensor
Pressure	Campbell CS105	Young 61202
O_3	UV photometry TE 49C	UV photometry TE 49C
NO, NO_2	Chemiluminescence TE 42C	Chemiluminescence TE 42C
CO	Gas-filter correlation TE 48C	Gas-filter correlation TE 48C
SO2	Pulsed Fluorescence TE 43C	Pulsed Fluorescence TE 43C
Photolysis rates	SAFS (JHONO, JNO_2, JO_3)	JNO_2 Radiometer
HONO	Wet-chemical photometry LOPAP3	-
VOCs	PTR-MS	PTR-MS
O_3 Vertical Profile	Ozonesondes	Ozonesondes
Column O_3, NO_2, HCHO	PANDORA	PANDORA

Table 4.1. Measured meteorological and chemical variables at Moody Towers and Smith Point, TX.

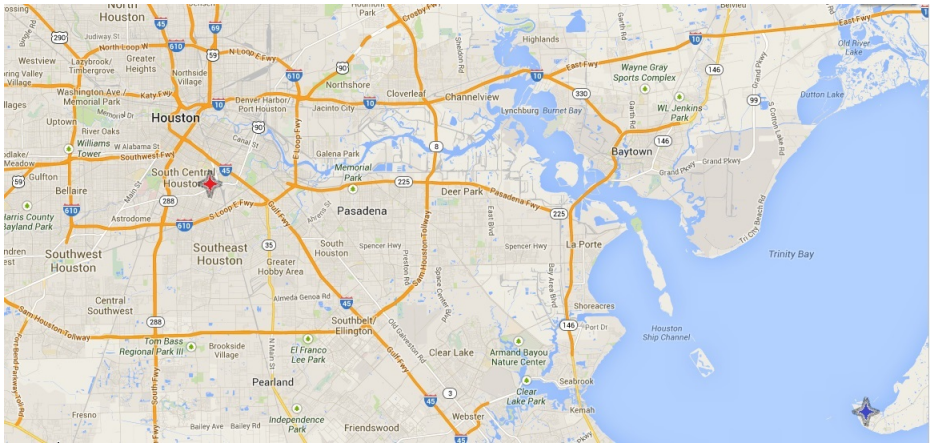

Fig. 4.1. Locations of MOPS1 and MOPS2 in Smith Point, TX (blue) and University of Houston's Moody Tower (red) (Google, 2013).

4.1 MOPS2 $P(O_3)$ Moody Towers Residence Hall: Houston, TX

The DISCOVER-AQ field campaign in Houston, TX was characterized by relatively low amounts of ozone for the majority of the campaign length, with very few days of ozone exceeding EPA NAAQS. The Penn State University MOPS2 obtained real-time instantaneous $P(O_3)$ measurements from Moody Towers for the entirety of the DISCOVER-AQ campaign. MOPS2 measurements from 13 September to 28 October 2013 are given in Figure 4.2.

On average, MOPS2 $P(O_3)$ maxima ranged from 20-40 ppbv hr^{-1} throughout the DISCOVER-AQ campaign. Recall that HONO may introduce a positive bias of about 15 ppbv hr^{-1}, so the actual $P(O_3)$ may be lower by 15 ppbv hr^{-1}. Consistent with low daily measured $P(O_3)$ rates, typical daily ozone maxima between 40-60 ppbv were measured for the Moody Tower North site. A likely cause for some of the observed low ozone

mixing ratios and production rates can be explained by morning southeasterly winds that transported relatively cleaner air from the Gulf of Mexico. Greater magnitudes of MOPS2 $P(O_3)$ rates are measured with morning north to northwesterly winds originating from the Houston metropolitan area (Figure 4.3).

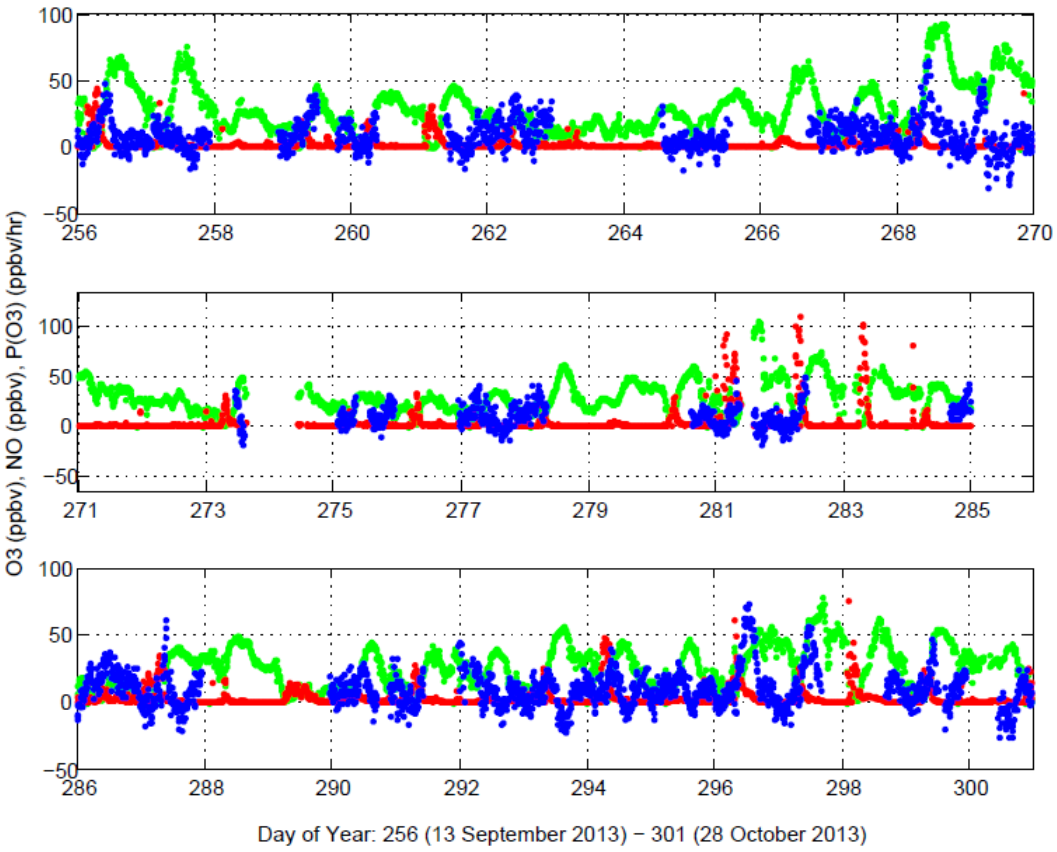

Fig. 4.2. MOPS2 (blue) ozone production rates for Moody Tower North in ppbv hr^{-1} and corresponding NO(red) and ozone (green) in ppbv.

Overall, the MOPS2 instantaneous measured ozone production rates are consistent with the ambient ozone experienced in the Houston region. MOPS2 $P(O_3)$ generally

peaks from 0930-1200 hours and begins to decrease later in the afternoon when NO mixing ratios reach a few ppbv. In most cases, high $P(O_3)$ was correlated with high nitric oxide mixing ratios.

This diurnal behavior is similar to that found in prior field studies conducted in the Houston area. For instance, in the summer 2006 TRAMP field study, the calculated ozone production rate peaks at 0930 and lasts for approximately three hours before decreasing later in the day (Chen et al., 2010). Similar results are reported in Mao et al. (2010) where calculated $P(O_3)$ peaks during the same hours and then decreases later in the day. In Mao et al. (2010), the ozone production sensitivity transit from VOC-sensitive to NO_x-sensitive occurs in the morning around the 1030 hour and then becomes VOC-sensitive again after 1500 hours. Similar ozone production sensitivity behavior during the spring 2009 SHARP campaign with $P(O_3)$ sensitivity transitioning from VOC-sensitive to NO_x sensitive regimes at the 1000 hour. For the spring 2009 SHARP campaign, modeled $P(O_3)$ peaks around noon, while the MOPSv1.0 measured $P(O_3)$ peaks around the hours from 0930-1200. In addition, it was found that for days with ozone mixing ratios greater than 70 ppbv, the transition from VOC-sensitive to NO_x-sensitive regimes occurred about three hours later than days when the ozone mixing ratio was less than 50 ppbv (Ren et al., 2013). It is likely that the MOPSv2.0 production sensitivity during the DISCOVER-AQ field campaign exhibits similar behavior to these prior Houston studies where $P(O_3)$ is VOC-sensitive in the morning hours before 1030 hours and NO_x-sensitive in the afternoon hours. Because the majority of the ozone production occurs between the hours of 0930-1200, these results may indicate that NO_x control may be an efficient summer approach to ozone mitigation in the Houston region.

The MOPS2 occasionally measured negative ozone production rates from 0 to -20 ppbv hr^{-1} in the afternoon hours. Likely explanations for these negative values are attributed to ozone analyzer zero drift fluctuations, possible imbalances between the sample and reference chambers and the inability of the current ozone analyzer to consistently and precisely measure these imbalances.

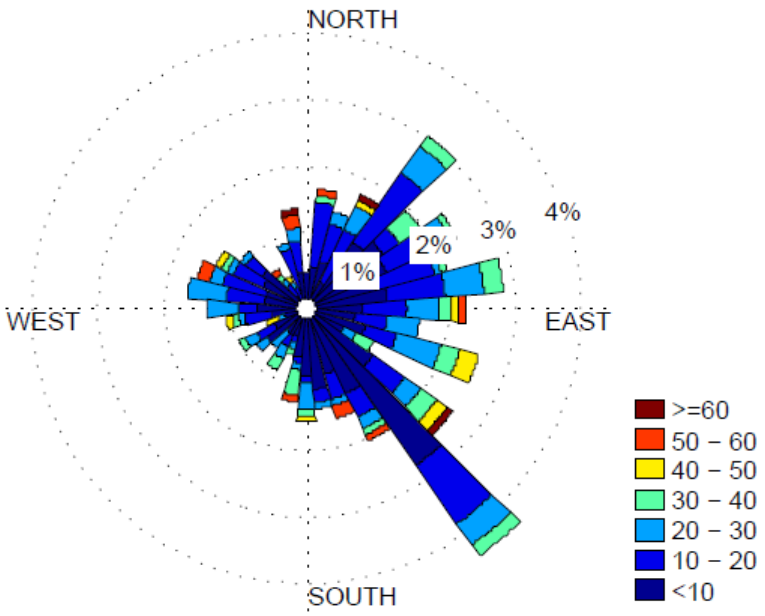

Fig. 4.3. MOPS2 ozone production rates as a function of wind direction, limited to daytime hours (CDT) from 0600 - 1500 for 13 September - 28 October 2013. Wind barb magnitudes represent percentages of the total wind originating from a given direction, while production rate magnitudes are shown in color.

4.2 MOPS1 P(O_3): Smith Point, TX and Moody Tower North

The MOPS1 was located on the roof of Penn State's NATIVE trailer at the DISCOVER-AQ Smith Point measurement site for 1 September 2013 to 1 October 2013. Again, despite the close proximity of this location to the adjacent Houston ship channel, unseasonably low amounts of ozone and its precursors were measured. Relatively clean conditions such as the low ozone and NO_x mixing ratios are likely due to easterly winds originating from the Gulf of Mexico for a majority of the DISCOVER-AQ campaign at Smith Point (Figure 4.4), which bring cleaner, less polluted air to the measurement site.

The MOPS1 field data collected both at Smith Point, TX from 13 September - 1 October 2013 and at Moody Tower North from 1 - 28 October are shown in Figure 4.5 with corresponding O_3 and NO mixing ratios. Even lower amounts of nitric oxides were measured at Smith Point, TX than at Houston, TX. Because of this difference, the MOPS1 average P(O_3) was 10-30 ppbv hr^{-1} during the Smith Point measurement period. During the Smith Point deployment, a number of technical and hardware issues were experienced, which limited the amount of MOPS1 Smith Point data that was collected.

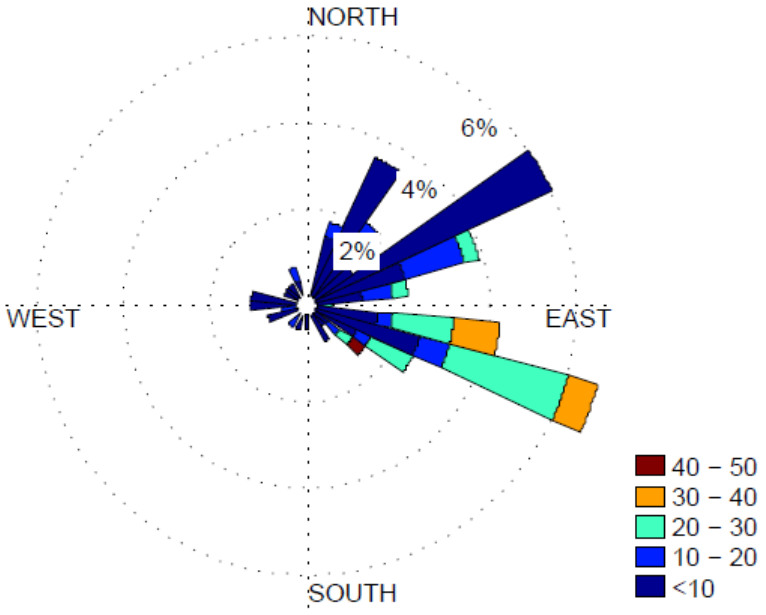

Fig. 4.4. MOPS1 ozone production rates as a function of wind direction, limited to daytime hours (CDT) from 0600 - 1500 for 13 September - 30 September. Wind barb magnitudes represent percentages of the total wind originating from a given direction, while production rate magnitudes are shown in color.

The MOPS1 also frequently measured $P(O_3)$ rates less than zero. Again, the MOPS1 negative afternoon $P(O_3)$ measurements are most likely caused by frequent drifting of the modified ozone analyzer zero which can be aggravated by variables such as high temperature and relative humidity changes and imbalances between the MOPS chambers.

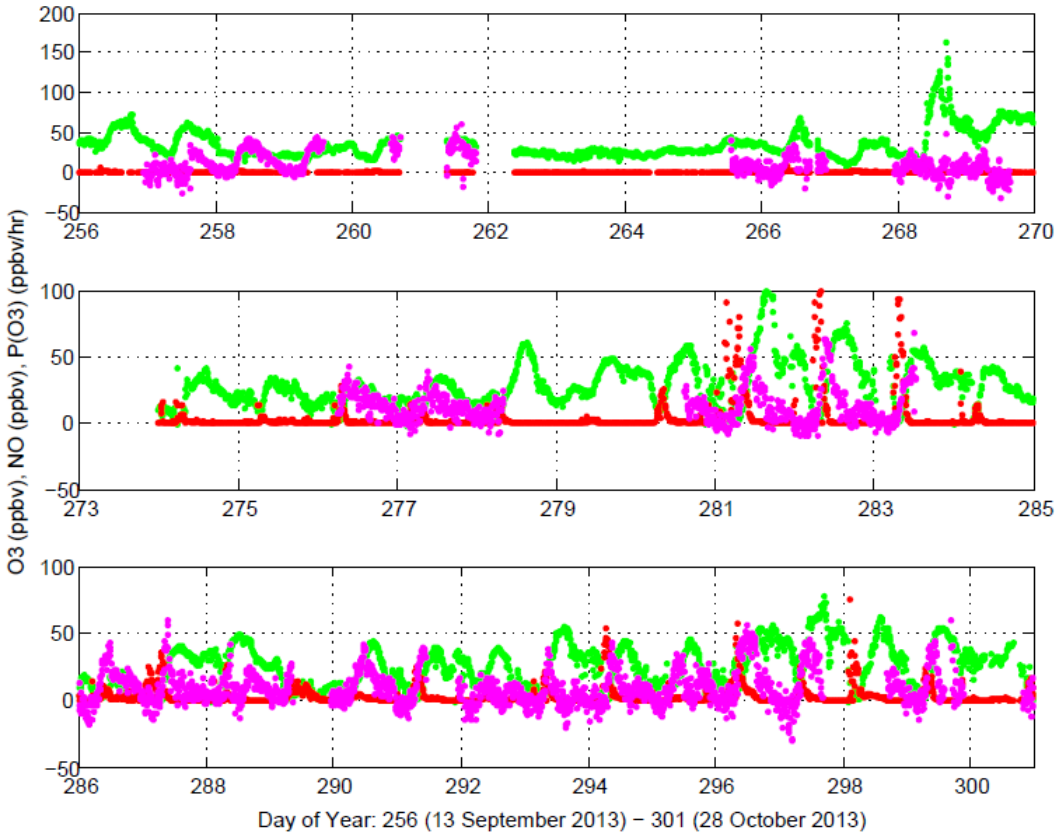

Fig. 4.5. MOPS1 (maroon) ozone production rates for Smith Point, TX (DOY<= 270) and Moody Tower North in ppbv hr^{-1} and corresponding NO(red) and ozone (green) in ppbv.

4.3 MOPSv2.0 Inter-comparison

One DISCOVER-AQ objective for the Penn State MOPSv2.0 was to compare the measurements of MOPS1 and MOPS2 while they were operating together at the Moody Tower site. A salient characteristic of the Penn State MOPS is its ability to calculate ozone advection and locate point sources of ozone so that it can help to evaluate the

efficacy of the EPA NAAQS. With MOPS1 and MOPS2 operating at different locations throughout the DISCOVER-AQ field campaign, an inter-comparison is required to justify that the measurements made between these two MOPSv2.0s are indeed the same. This comparison will also increase confidence in the MOPSv2.0 measurement process and zeroing techniques.

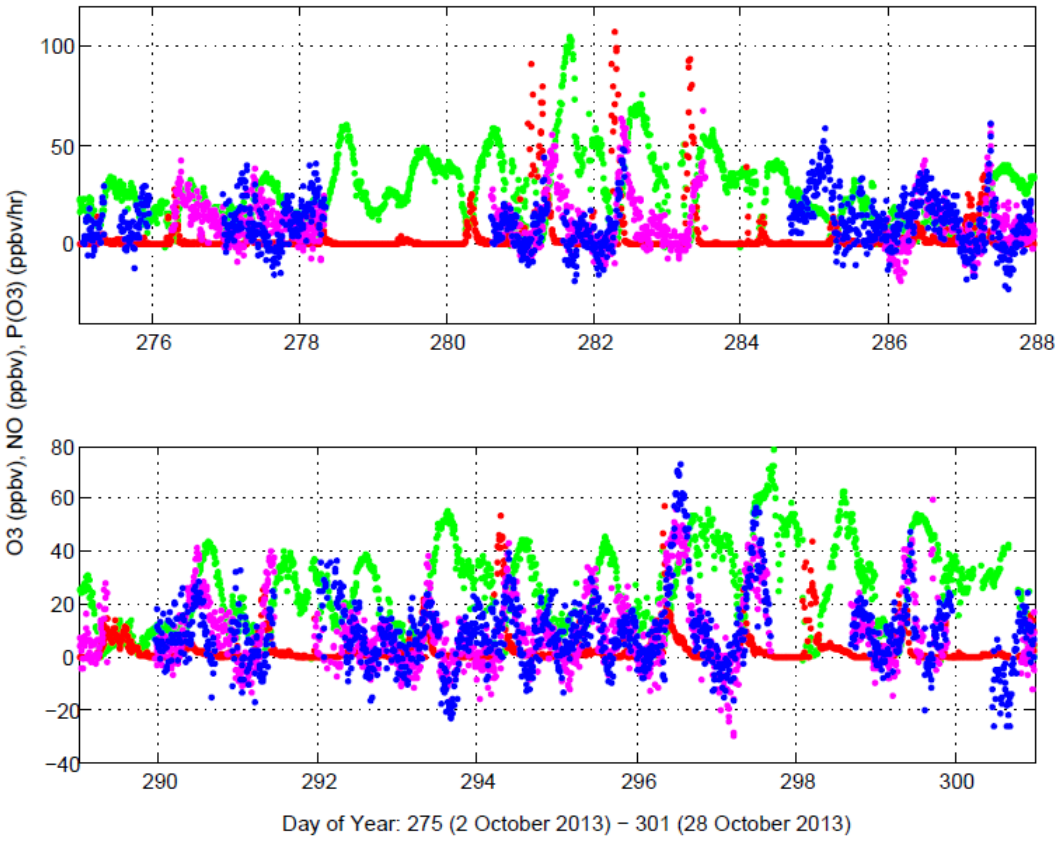

Fig. 4.6. MOPS1 (maroon) and MOPS2 (blue) field campaign data from 2 - 28 October 2013 located at Moody Tower, Houston, TX. Corresponding NO (red) and O_3 (green) are plotted.

The MOPS1 and MOPS2 simultaneous data collected at Moody Tower North from 2-28 October (DOY 275-301) is shown in Figure 4.6. During this period, the MOPSv2.0s obtained automated $P(O_3)$ measurements without human interference or chamber zeroing, which gives confidence in the new version of the MOPS to provide continuous real-time $P(O_3)$ measurements when it is operating in a stand-alone environment or in a network of multiple MOPSv2.0s.

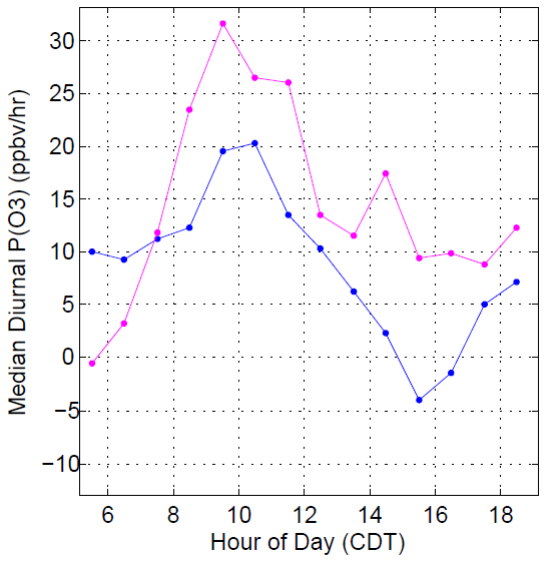

Fig. 4.7. MOPS1 (maroon) and MOPS2 (blue) median diurnal $P(O_3)$ from 2 - 28 October 2013 located at Moody Tower, Houston, TX. Hour of day (CDT) is restricted to between 0500 and 1800 hours.

The co-located MOPS1 and MOPS2 $P(O_3)$ measurements at Moody Tower North provide similar median diurnal patterns with $P(O_3)$ hourly trends consistent in both MOPSv2.0s (Figure 4.7). Both MOPS1 and MOPS2 median diurnal $P(O_3)$ peak from

roughly 0930-1200 hours and agree to within 15 ppbv hr^{-1} of each other throughout the day. Although MOPS1 $P(O_3)$ exhibited consistently higher values by 10 ppbv hr^{-1}, the consistent diurnal behavior between the MOPSs indicates that this occurrence may be explained by inconsistencies in either the ozone analyzer zero drifts or chamber zero correction methods between the two instruments. Continued chamber zero characterization and further reduction of this zero drift can help to minimize these differences.

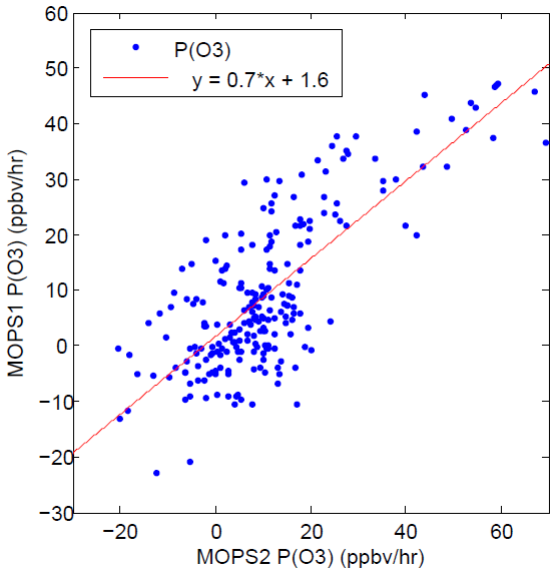

Fig. 4.8. MOPS1 and MOPS2 data correlation for DOY 293-298 at Moody Tower North, Houston, TX ($R^2 = 0.59$).

An R^2 value of 0.59 was calculated between the MOPS1 and MOPS2 data from 20-28 October (DOY 293-298) when both MOPSv2.0s took continuous measurements without chamber zeroing (Figure 4.8). Again, this coefficient of determination is expected to be low because of differences in zero drifts and chamber zeroing between the

two MOPSs. All in all, the consistent measurements between both MOPSs implies that the MOPSv2.0 measurement processes and zeroing methods are the same and produce similar $P(O_3)$ values. The above comparison suggests that the negative $P(O_3)$ measurements at the Moody Tower site are not random but, instead, arise from systematic errors either in the modified ozone analyzer or in the measurement environment.

4.4 MOPSv2.0 Validation

Further validation of the MOPSv2.0 measurement is provided with comparisons to MOPSv1.0 measurements conducted in Houston, TX in 2006 (Figure 4.9). The instantaneous ozone production rate in Equation 1.1 is constrained by NO as well as the production of HO_x ($P(HO_x)$), where $HO_x = OH + HO_2$ (Ren et al. (2013), Ren et al. (2003). $P(HO_x)$ begins to increase between the hours of 0600 and 0900, grows rapidly until noon where it levels off, and then decreases during the afternoon hours (Ren et al., 2013). Although the MOPSv2.0 measurement is not accompanied by modeled or calculated $P(O_3)$ with HO_x and RO_2 species, the MOPSv2.0 $P(O_3)$-NO dependence exhibits diurnal trends similar to the MOPSv1.0 measured, calculated, and modeled $P(O_3)$ diurnal trends assuming that $P(HO_x)$ levels during DISCOVER-AQ are comparable to those in the 2006 TRAMP field campaign (Figure 4.9).

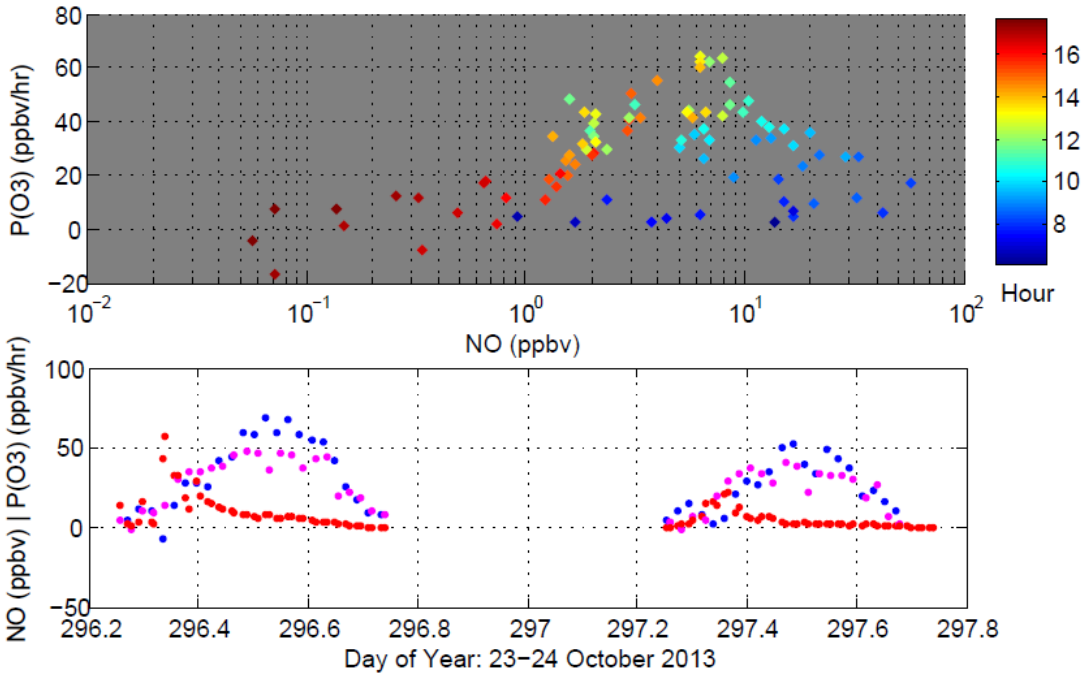

Fig. 4.9. MOPS1 and MOPS2 $P(O_3)$ (ppbv hr^{-1}) versus NO. The hour of day is indicated by color as in Cazorla et al. (2012). Hours (CDT) from 0700 - 1800 are plotted. The time series of $P(O_3)$ for MOPS1 (maroon), MOPS2 (blue), and NO (ppbv, red) were measured at the Moody Tower North, Houston, TX site and are plotted for hours 0600-1800.

The measured $P(O_3)$ levels can be compared to measured and calculated $P(O_3)$ from the same site. For instance, like Cazorla et al. (2012), the MOPSv2.0 $P(O_3)$ curves begin at high NO with production rates below 20 ppbv hr^{-1} around 0700-0900 hours when $P(HO_x)$ is small. After the 0900 hour, $P(HO_x)$ is expected to rapidly increase as NO falls throughout the morning rush hour, and production rates increase rapidly from 20-60 ppbv hr^{-1} until 1200 hours. Then, $P(O_3)$ peaks and levels off with $P(HO_x)$ when NO reaches approximately 2-5 ppbv in later morning hours, and then decreases

in the afternoon as NO and HO_x production decreases. According to other field studies conducted in urban plumes (Martinez et al. (2003),Ren et al. (2013)), $P(O_3)$ is expected to peak at lower NO mixing ratios around 1-2 ppbv, and then decrease with higher NO. However, the MOPSv2.0 $P(O_3)$ peaks at higher NO than suggested. On 23 October, $P(O_3)$ peaks between 3-7 ppbv of NO, whereas on 24 October, $P(O_3)$ peaks at the expected level of NO around 1 ppbv. Thornton et al. (2002) suggests that the NO mixing ratio where $P(O_3)$ stops increasing linearly with NO and levels off shifts to higher values as $P(HO_x)$ increases, which may suggest that 23 October experienced higher $P(HO_x)$ than 24 October. Because measured to modeled HO_2 ratios are still in disagreement at high NO, more research is needed to confirm these results.

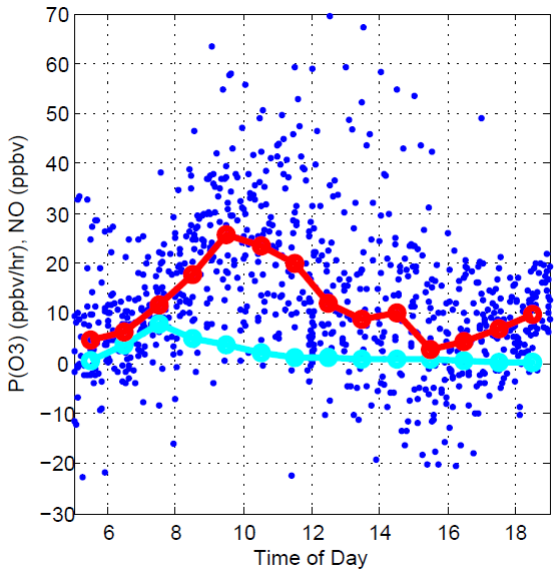

Fig. 4.10. Averaged median diurnal $P(O_3)$ profile for MOPS1 and MOPS2 data (red) and median diurnal NO (cyan). $P(O_3)$ measurements for MOPS1 and MOPS2 are shown in blue for 2 - 28 October 2013. The time of day is limited to daylight hours between 0500 and 1800.

Additional comparison of the MOPSv2.0 $P(O_3)$ to measured, modeled, and calculated $P(O_3)$ from prior Houston, TX field data (Ren et al. (2013), Chen et al. (2010)) can provide yet another check for the MOPSv2.0 measurement. Figure 4.10 presents raw campaign data from 2-28 October for MOPS1 and MOPS2, as well as the MOPS1 and MOPS2 averaged median diurnal instantaneous ozone production rate and median NO diurnal mixing ratio. The MOPSv2.0 instantaneous ozone production rate exhibits similar diurnal trends compared to previously calculated Moody Tower (TRAMP, 2006) instantaneous $P(O_3)$ from measured HO_2 radicals in Chen et al. (2010). $P(O_3)$ increasing around 0800 hours, leveling off between 1000 and 1200 hours, and then decreasing with decreasing NO and $P(HO_x)$ in the afternoon hours.

The MOPSv2.0 median diurnal $P(O_3)$ is also fairly consistent with modeled $P(O_3)$ from SHARP field data in 2009. For approximately 5-10 ppbv of NO, the MOPSv2.0 median diurnal $P(O_3)$ is within 10% of the measured MOPSv1.0 $P(O_3)$ (25 ppbv hr^{-1}) at 1000-1100 hours. The MOPSv2.0 $P(O_3)$ peak is approximately one hour before the $P(O_3)$ peak from calculated HO_2 and RO_2 radicals but is almost twice as high (Ren et al., 2013). Without the additional 15 ppbv hr^{-1} positive bias that HONO production within the chambers introduces, the MOPSv2.0 $P(O_3)$ would agree with the calculated $P(O_3)$ to within 30%.

As mentioned in Chapter 3 and emphasized in Figure 4.10, the need to decrease the potential HONO bias and limit of detection is salient for producing a quantitative MOPSv2.0 $P(O_3)$ measurement. Decreasing these sources of error can be done through extended HONO analysis and further reduction in the modified ozone analyzer zero drift. These comparisons to prior Moody Tower North field campaign data give confidence in

the MOPSv2.0 development, measurement process, and potential to contribute to ozone chemistry by constraining chemical mechanisms in air quality models.

4.5 MOPSv2.0 Assessment of Ozone Advection: 25 September 2013

One feature of the MOPSv2.0 is its ability to directly assess ozone transport using the ozone budget equation, Equation 1.2. As the local change in ozone, $\frac{\partial O_3}{\partial t}$, can be determined from commercial ozone analyzer measurements and $P(O_3)$ is directly measured by the MOPSv2.0, it is now possible to quantitatively assess the ozone advection rate near the surface because of our ability to isolate the instantaneous ozone production rate. By subtracting $P(O_3)$ plus the O_3 deposition rate from $\frac{\partial O_3}{\partial t}$, we can directly calculate the surface ozone advection rate at any MOPS location. Typical ozone deposition rates are assumed to be on the order of 1-2 ppbv hr^{-1} based on an average boundary layer depth of 500m, an ozone mixing ratio of 40 ppbv and an ozone deposition velocity of 0.5 cm s^{-1}. Since the ozone deposition term is small and MOPSv2.0 measures only $P(O_3)$, this term is neglected when calculating the ozone advection rate. One example is given with a high ozone event experienced in Houston, TX on 25 September 2013.

During the morning hours of 25 September 2013, MOPS2 measured $P(O_3)$ rates exceeding 50 ppbv hr^{-1} at times between 0900-1200 hours at Moody Tower while the change in ozone was only 40 ppbv, or 14 ppbv hr^{-1} (Figure 4.11, top panel). At this location, high morning $P(O_3)$ rates were associated with nitric oxide mixing ratios around 20 ppbv and with northwesterly flow from the greater Houston metropolitan region. $P(O_3)$ peaked during the 1100 hour at approximately 60 ppbv hr^{-1} as NO decreased.

After noon as winds switch from northwesterly to northeasterly flow, measured $P(O_3)$ rates were less than 25 ppbv hr^{-1}.

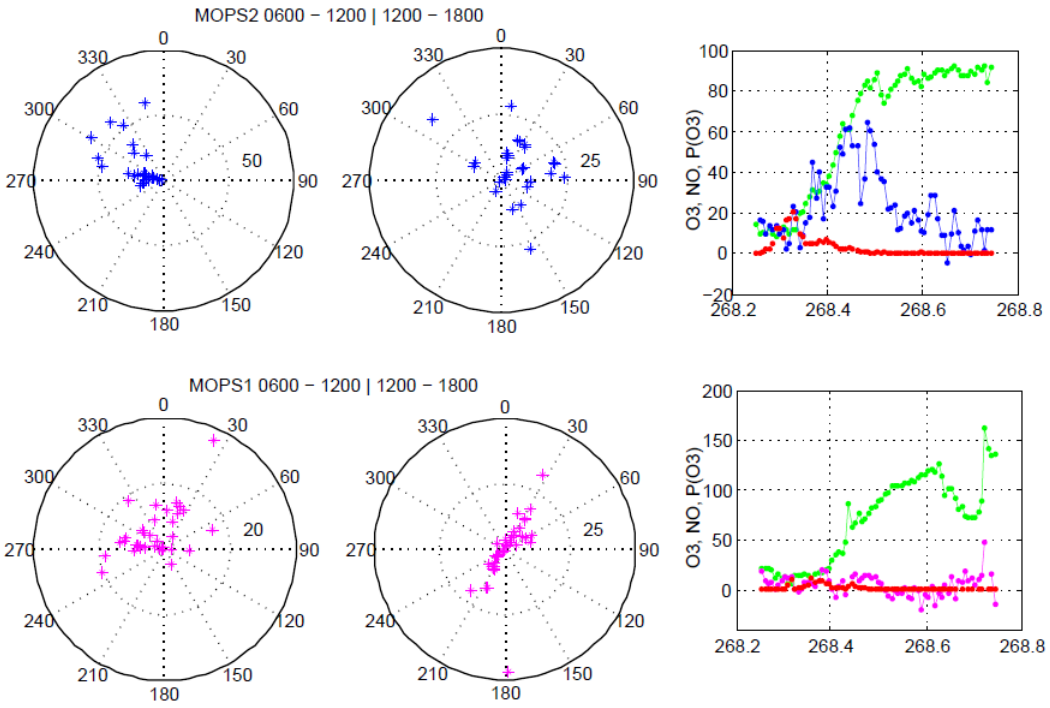

Fig. 4.11. High ozone event experienced 25 September 2013 in Houston, TX. MOPS1 and MOPS2 Smith Point and Moody Tower $P(O_3)$ (ppbv hr^{-1}) as a function of wind direction is shown in maroon and blue for hours 0600-1200 (left), and 1200-1800 (middle). Corresponding time series of MOPS1 and MOPS2 $P(O_3)$ (ppbv hr^{-1}) with NO(ppbv, red) are shown on the far right.

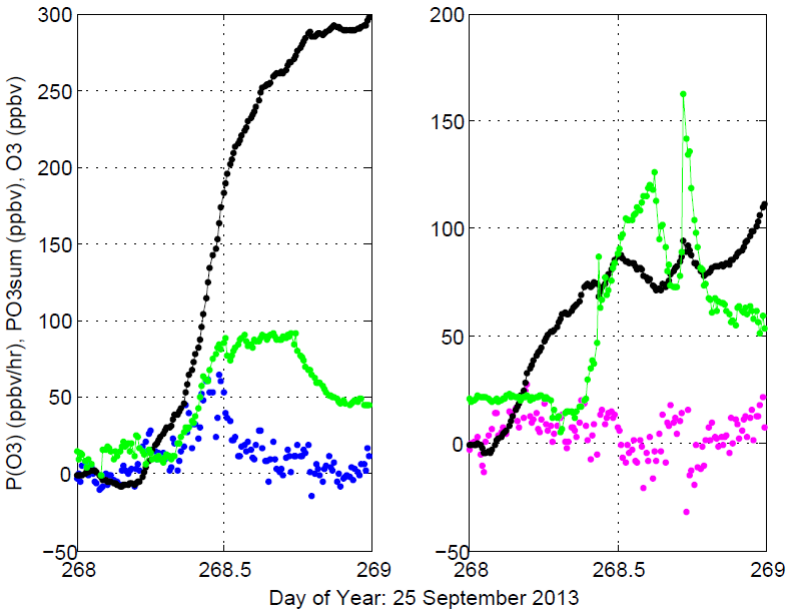

Fig. 4.12. Moody Tower North and Smith Point cumulative ozone production, PO3sum, (black) , ozone (green) and measured $P(O_3)$ for 25 September 2013. The MOPS2 Moody Tower $P(O_3)$ measurement case (blue) is shown on the left, the MOPS1 Smith Point $P(O_3)$ case (maroon) is on the right.

The MOPS2 Moody Tower and MOPS1 Smith Point measured $P(O_3)$ and ozone mixing ratio as well as the corresponding cumulative ozone production calculated for each measurement site is shown in Figure 4.12. For this location, the total accumulated ozone production for 25 September was approximately 300 ppbv. The ozone advection rate for a certain time period is derived from the difference between the local rate of change of ozone and the MOPS $P(O_3)$ (Figure 4.13). For the Moody Tower location, $\frac{\partial O_3}{\partial t}$ is smaller than $P(O_3)$ for much of the day. In particular, the average morning (0600-1200 CDT) ozone advection rate is approximately -20 ppbv hr^{-1}. This negative rate indicates that

air with less ozone is being transported to the Moody Tower site. Because the horizontal winds were northwesterly during the morning hours when the ozone production rate was the largest, it is likely that the majority of the ozone produced at Moody Tower was advected elsewhere and that Moody Tower was amidst an ozone production location in the Houston region. In the afternoon (1200-1800 CDT), the average ozone advection rate is -15 ppbv hr^{-1}, which again indicates that air with less ozone was being transported to the measurement site. The total decrease in $\frac{\partial O_3}{\partial t}$ due to advection between 0600-1800 hours was calculated to be 210 ppbv.

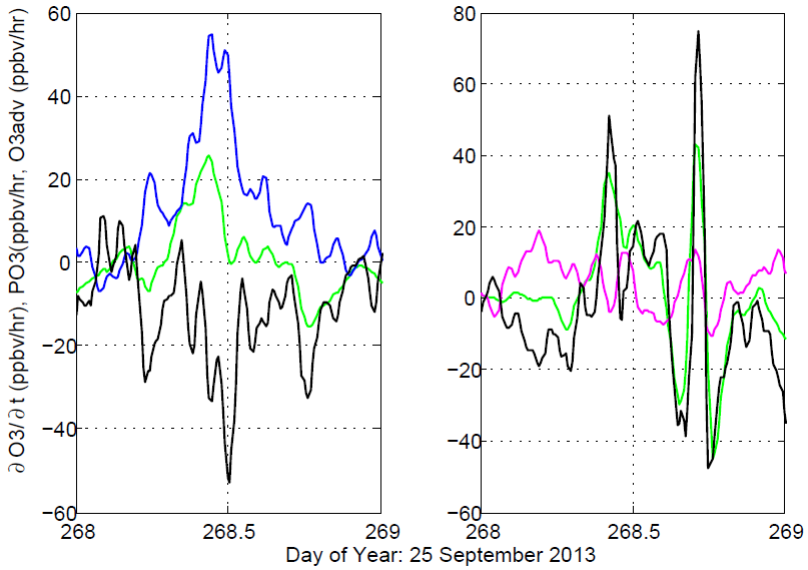

Fig. 4.13. Moody Tower North (left) and Smith Point(right) PO_3, advection rate (black), and local rate of change of ozone (green).

MOPS1 $P(O_3)$ rates measured in Smith Point, TX were less than 20 ppbv hr^{-1} with northwesterly winds between 0600 - 1200 (Figure 4.11, bottom panel). Low MOPSv2.0

measured $P(O_3)$ was consistent with nitric oxide mixing ratios less than 10 ppbv throughout the early morning hours. Afternoon $P(O_3)$ rates were less than 20 ppbv hr^{-1}, while ozone mixing ratios increased to over 100 ppbv. Later in the day, ozone mixing ratios greater than 100 ppbv and even 150 ppbv were measured. As the cumulative ozone production, PO_3sum was approximately 110 ppbv (Figure 4.12), this indicates that a substantial amount of ozone was advected to the Smith Point location.

HYSPLIT (Hybrid Single Particle Lagrangian Integrated Trajectory) ensemble forward trajectories in Figure 4.14 initiated at 1200 UTC (0700 CDT) along with Figure 4.11, depict the onset of a bay breeze event later in the day where southwesterly winds recirculated polluted air to the Smith Point location (Draxler and Rolph, 2014). The bay breeze event effectively brought ozone amounts greater than 150 ppbv to Smith Point, TX later in the afternoon of 25 September.

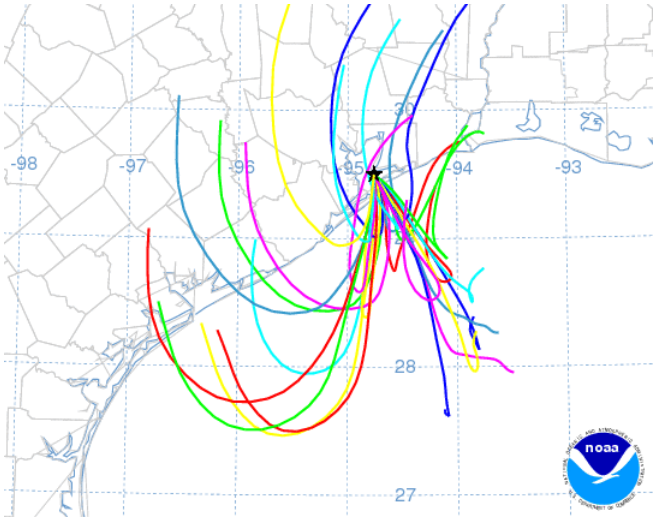

Fig. 4.14. HYSPLIT forward trajectory initiated at 1200 UTC on 25 September 2013 in Smith Point, TX and run for 24 hours. HYSPLIT trajectories obtained 20 October 2013 from: http://www.arl.noaa.gov/HYSPLIT.php (Draxler and Rolph, 2014).

The Smith Point measurement site experienced very little ozone production throughout the day, and so the local change in ozone was dominated by ozone transport rather than ozone production. The average calculated ozone advection rate away from the site for the morning hours between 0600-1200 hours is approximately -5 ppbv hr^{-1} (Figure 4.13). During this period, the average $\frac{\partial O_3}{\partial t}$ is approximately equal to the average PO_3, which suggests that there was little to no change in ozone due to advection. Between 1200-1400 hours, an increase in the local ozone from approximately 80 ppbv to over 120 ppbv is measured along with a calculated average ozone advection rate of +20 ppbv hr^{-1} to the site. Thus, it is likely that the northeasterly horizontal wind is bringing ozone-rich air to the Smith Point site (Figure 4.11). As the bay breeze brings polluted air back to the Smith Point site, a sharp spike in the local ozone at 160 ppbv is measured at

1715 hours. The average calculated ozone advection rate from 1700-1800 is +50 ppbv hr^{-1}. This MOPSv2.0 advection analysis suggests that, because very little $P(O_3)$ was measured, the morning $\frac{\partial O_3}{\partial t}$ was not influenced by ozone advection, while the afternoon ozone was dominated by ozone transported to the site and re-circulated back to Smith Point through the bay breeze event later in the day.

Chapter 5

Conclusions

The recently developed second version of the Penn State Measurement of Ozone Production Sensor, MOPSv2.0 improves upon the component limitations, measurement technique, and chamber flow regime of the previous MOPSv1.0. The MOPSv2.0 has been successfully deployed in the 2013 DISCOVER-AQ summer field campaign in Houston, TX and its potential to contribute to ozone chemistry has been tested. Although more work is needed to reduce the limit-of-detection and potential biases in the MOPSv2.0 measurement, much has been learned from the Houston deployment, and the results presented are promising.

5.1 Summary

The Penn State Measurement of Ozone Production Sensor provides the first direct measurement of the ambient ozone production rate. The MOPSv1.0 provided a first test of atmospheric oxidation chemistry but had routinely measured negative ozone production rates at midday, which can stem from interactions with sampled air and the chamber walls. Although the MOPSv1.0 provided a first comparison to both calculated and modeled $P(O_3)$, extensive laboratory testing was required to provide confidence in these new measurements and to draw conclusions from the MOPSv1.0 results. A primary goal in developing a second version of the MOPS is to help us to continue to test

the improvement of the MOPS technique with a newer, more robust and automated instrument that has minimized chamber wall effects. With the development of a second version, MOPSv2.0, the MOPS is almost ready to tackle its primary goals in air quality studies: to determine where air quality model output and chemical mechanisms succeed and fail, to aid in the design of air quality standards for mitigating ozone pollution, and to provide a direct $P(O_3)$ measurement for assimilation into air quality simulation models.

The MOPSv2.0 is a significant improvement over the MOPSv1.0. In particular, MOPSv2.0 is more robust, fully automated and more thoroughly studied for possible interferences. This improved performance comes from several changes including the following:

- Changes in the shape and size of the chamber to mechanically force air from the entrance to the exit regions of the chamber
- Addition of chamber components that preserve laminar flow such as an open-faced inlet and various laminar mesh screens
- Formulation of a sheath flow regime with faster, exhausted air on the walls of the chambers and slower, sampled air in the center
- Increased stability via a heating-grid induced, vertical temperature gradient within the chamber
- Full automation of the MOPSv2.0 operation via LabView control
- A highly efficient NO_2-to-O_3 converter

- The addition of DewLines® to decrease water vapor interferences within the commercial ozone analyzer.

Full automation of the MOPSv2.0 allows for real-time, continuous measurements without human operation. With the ability to monitor over 50 variables, technical and communication errors are minimized, while characterization of the MOPSv2.0 is much more comprehensive than the first version. The inclusion of a highly efficient UV LED converter unit allows for over 90% conversion of NO_2 at values less than 20 ppbv and over 75% conversion of NO_2 at values over less than 110 ppbv, an improvement over the previous MOPSv1.0 NO_2 converter by over 5% at NO_2 less than 20 ppbv and over 10% at NO_2 between 40-100 ppbv. Case studies and photochemical box model characterization of the converter unit show that this decreases the NO_x PSS differences between the two chambers to less than 0.2 ppbv hr^{-1}, with less than a 15% bias for Houston, TX NO_2 to O_3 ratios. Further model analysis of the efficiency of the converter unit in different NO_x and ozone regimes yields less than a 15% error for typical Houston morning, midday, and afternoon atmospheric conditions.

Preliminary measurements obtained of nitrous acid in the MOPSv2.0 chambers provides insight into the potential HONO photochemical effects on the $P(O_3)$ measurement. Due to differences in photolysis between the sample and reference chamber, the sample chamber experiences an added HONO source that is expected to stem from photo-enhanced production of HONO from photolysis of NO_2 that has been adsorbed to chamber surfaces. Photochemical box model simulations of this HONO source in the

sample chamber result in a potential 15 ppbv hr^{-1} positive bias under illuminated conditions, and less than a 5 ppbv hr^{-1} bias for Ultem-covered conditions. High confidence in the heating grid ability to stabilize the chamber flow and deter wall interactions localizes the HONO production near the entrance surfaces of the MOPSv2.0 chambers, although more testing is needed to verify this hypothesis. From preliminary results, it is expected that shading the MOPSv2.0 entrance region can suppress this photoenhanced HONO artifact without compromising photolytic effects on the chamber chemistry.

New procedures and zeroing methods preceding the derivation of the MOPSv2.0 ozone production rate include new approaches to tracking the ozone analyzer zero – cycling flow between ambient and MOPS chamber air – which makes the MOPSv2.0 measurement more robust and objective while creating an automatic ozone analyzer zero every five minutes. In addition, applying frequent chamber zeros to the $P(O_3)$ measurement helps to correct for any imbalances between the sample and reference chamber. The MOPSv2.0 absolute limit of detection is estimated to be 15 ppbv hr^{-1}, which is sufficient enough to measure ozone production in urban environments but is not currently sufficient enough to measure $P(O_3)$ in cleaner, more remote atmospheres. Limitations in the MOPSv2.0 detection primarily arise from fluctuations in the modified ozone analyzer zero drift. These limitations in the ozone analyzer are the largest source of uncertainty in the MOPSv2.0 ozone differential measurement and directly affect the MOPSv2.0 absolute error. The ozone differential is used for the MOPSv2.0 error propagation analysis yielding an absolute error in the ozone differential of 1.5 ppbv per five minute cycle time. This corresponds to a standard deviation in the MOPSv2.0 measurement of 20 ppbv hr^{-1}, respectively.

The MOPSv2.0 was deployed in Houston, TX for the "Deriving Information on Surface conditions from Column and Vertically Resolved Observations Relevant to Air Quality" (DISCOVER-AQ) field campaign from mid-August to 28 October 2013. Increased HONO production within the MOPS chambers can positively bias the $P(O_3)$ measurement 15 ppbv hr^{-1} and so the MOPSv2.0 $P(O_3)$ rate may actually be lower by 15 ppbv hr^{-1}. These field results are a first test of the MOPSv2.0 measurement and data analysis techniques. In addition, they demonstrate the benefit of adding the MOPSv2.0 – or a network of MOPSv2.0s – to air quality networks in order to assess $P(O_3)$ dependence on NO_x and VOCs under $P(HO_x)$ conditions, to locate ozone point sources, and to calculate ozone advection.

Two MOPSv2.0s, MOPS1 and MOPS2, were deployed to Houston, TX where they obtained continuous $P(O_3)$ measurements. MOPS2 was stationed at Moody Tower North on the University of Houston campus, while MOPS1 was located at Smith Point, TX from September to October. A final inter-comparison of both MOPS1 and MOPS2 performance took place at Moody Tower North from 4-28 October 2013.

The DISCOVER-AQ field campaign was characterized by unseasonably low ozone concentrations at both Moody Tower and Smith Point sites due to cleaner air originating from the Gulf of Mexico. Consequently, the MOPS1 and MOPS2 measured lower ozone production rates. At Moody Tower, MOPS2 generally exhibited lower $P(O_3)$ measurements between 20-40 ppbv hr^{-1} consistent with the ozone concentrations (40-60 ppbv) experienced at the measurement site. Increased $P(O_3)$ was experienced in the presence of high NO_x concentrations and northwesterly winds originating from the Houston

metropolitan region. The MOPS2 DISCOVER-AQ $P(O_3)$ maxima occur at approximately the same hour of day as previous studies (TRAMP 2006 and SHARP 2009) at Moody Towers (Ren et al. (2013), Chen et al. (2010), Mao et al. (2010)). From these prior field analyses of ozone production sensitivity, the transition from VOC-sensitive to NO_x-sensitive regimes occurs during the morning hours between 10-1030 hours. Because the majority of ozone production occurs between 0930-1200, NO_x control may be a viable solution to ozone mitigation during the Houston summer.

The MOPS1, located in Smith Point, TX exhibited similar $P(O_3)$ patterns consistent with lower daily ozone concentrations. Primarily easterly winds originating from the Gulf of Mexico brought cleaner, less polluted air to the Smith Point measurement site, where $P(O_3)$ was generally less than 30 ppbv hr^{-1} and ozone concentrations were less than 50 ppbv. The MOPS1 Smith Point, TX data is limited because of greater amounts of hardware issues that occurred during this time.

Some discrepancies are still evident in the MOPS1 and MOPS2 zero, which frequently create negative afternoon ozone production rate measurements. This can be corrected for with further analysis of differences between the sample and reference chambers as well as with a reduction in the modified ozone analyzer zero drift fluctuations.

MOPS1 and MOPS2 simultaneous measurements were made from 1-28 October at Moody Tower North. In general, both MOPS1 and MOPS2 exhibited similar diurnal trends and measured $P(O_3)$ was within 15 ppbv hr^{-1} between the two instruments. MOPS1 $P(O_3)$ were consistently higher by 10 ppbv hr^{-1}, which could be explained by inconsistencies between the MOPS1 and MOPS2 ozone analyzer zero drifting and zeroing corrections. An R^2 value of 0.59 was calculated for a time period when both MOPSs

measured continuous $P(O_3)$ without any chamber zeroing. The similarity between the MOPS1 and MOPS2 measurements further validate the use of the chamber zeroing technique as well as increase confidence in the ability for several MOPSv2.0s to make consistent, comparable measurements in a network.

Although the MOPS1 and MOPS2 $P(O_3)$ measurements were not binned according to $P(HO_x)$, the ozone production rate in NO space was compared to previous MOPSv1.0 $P(O_3)$ in NO space for further validation of measurement techniques and zeroing methods. Similar to Cazorla et al. (2012), the instantaneous ozone production rate curves begin at high NO when $P(HO_x)$ is small, increase with $P(HO_x)$ and decreasing NO until approximately noon, level off, and then finally decrease with NO and HO_x production in late afternoon. Additional comparison of the MOPSv2.0 production rates to Houston, TX $P(O_3)$ from the SHARP 2009 field campaign show agreement with the MOPSv1.0 $P(O_3)$ to within 10%. Without the additional 15 ppbv hr^{-1} positive bias that HONO production introduces to the MOPSv2.0 measurement, MOPSv2.0 would agree to calculated $P(O_3)$ to within 30% (Ren et al., 2013).

An evaluation of a high ozone event (25 September 2013) highlights the capability for the MOPSv2.0 to directly calculate the instantaneous ozone advection rate. During the morning hours of 25 September 2013, MOPS2 measured $P(O_3)$ rates of exceeding 50 ppbv hr^{-1} at times at Moody Tower while the change in ozone from 0900-1200 was only 40ppbv. The net decrease in the local ozone from 1200-1800 hours due to advection was calculated to be 90 ppbv. Direct ozone advection calculations indicate that Moody Towers was amidst a region where the local change in ozone was dominated by local production. Meanwhile, low MOPS1 measured $P(O_3)$ at Smith Point was consistent

with nitric oxide mixing ratios less than 10 ppbv throughout the early morning hours. Afternoon $P(O_3)$ rates were less than 20 ppbv hr^{-1}, while ozone mixing ratios increased approximately 80 ppbv. The Smith Point site experienced a bay breeze event validated by HYSPLIT trajectories, which effectively brought ozone mixing ratios exceeding 150 ppbv to the measurement location. An ozone advection rate of +50 ppbv hr^{-1} was calculated between 1700-1800 in association with this bay breeze event. MOPSv2.0 advection analysis suggests that, because very little $P(O_3)$ was measured, the morning ozone was dominated by local production, while the afternoon ozone was dominated by ozone advection.

Further MOPSv2.0 network analyses of $P(O_3)$ and local meteorology can help to provide information about where ozone point sources are located and how much ozone is being transported to and from measurement sites. This current analysis examines the total advected ozone both horizontally and vertically at the surface. With extended instrumentation such as ozone LIDAR or sonic anemometers and analysis of local meteorology, the vertical ozone transport within the surface layer can be determined. The ability for the MOPSv2.0 to directly calculate ozone advection can be instrumental in determining whether ozone is transported to the surface from the residual layer or advected horizontally from other point sources. Future MOPSv2.0 network advection analyses can illuminate urban ozone source locations that should be regulated more closely by EPA NAAQS, as well as locate areas of environmental injustice.

5.2 Future Research

With the second stage of development in the Penn State MOPS comes a broader knowledge base of the instrument and ways for further improvement. In general, much has been learned about the MOPSv2.0 habits and operation and using photochemical box models to characterize possible bias and error within the MOPSv2.0 $P(O_3)$ measurement.

Reducing the largest source of error in the MOPSv2.0 involves decreasing the ozone analyzer zero drift fluctuations. The principle of detection in a UV photometric ozone analyzer such as one used in the MOPS system involves the use of photometry to measure the quanta of light reaching the ozone detector at 254nm. According to the Beer-Lambert Law, this measurement of the reduction of light due to ozone absorption at 254nm is based on the path length of the UV cell, the ozone concentration in the cell, and the wavelength of the UV light. The non-linear fluctuation in the zero drift is a key problem that is hypothesized to be reduced with further characterization and increased detection sensitivity (i.e., increased path length) in the ozone analyzer.

More work is needed to prove that the MOPSv2.0 chamber walls do not interfere with the sampled air that provides a basis for the $P(O_3)$ measurement. This effort involves extensive laboratory analysis and measurement of various constituents within the MOPSv2.0 chambers. As noted above, further research is needed to fully characterize and suppress the effects of HONO production in the MOPSv2.0 chambers.

Although it is possible to characterize the MOPSv2.0 through photochemical modeling of the chemical processes in each chamber, this method only gives an estimated uncertainty of the MOPS $P(O_3)$ measurement. A calibration method for the Penn State

Measurement of Ozone Production Sensor must be devised in order to verify the absolute uncertainty in the MOPS and obtain a more quantitative $P(O_3)$ measurement. Because the MOPSv2.0 inlet is open to ambient air, a proper way of injecting calibration mixtures must also be devised. While several studies have tested individual aspects of the MOPS performance, a calibration will provide an integrated test of performance and possible interferences.

A goal of the MOPSv2.0 is to provide assessment for air quality models and EPA model-derived abatement strategies. Testing of model output and chemical mechanisms can be achieved with comparison to MOPSv2.0 measured $P(O_3)$. Future work, and a near-term goal of the MOPSv2.0, is to demonstrate that assimilating $P(O_3)$ measurements in air quality simulation models will significantly improve air quality forecast models. The ultimate goal is to deploy MOPSs in air quality networks around the world to give better guidance to air quality managers on the best approaches to mitigate ozone pollution.

Bibliography

Baird, C. and M. C. Cann, 2008: *Environmental chemistry*. W.H. Freeman, New York, NY.

Berman, J. D., et al., 2012: Health benefits from large-scale ozone reduction in the united states. *Environmental Health Perspectives*, **120 (10)**.

Carter, W. P. and F. W. Lurmann, 1991: Evaluation of a detailed gas-phase atmospheric reaction mechanism using environmental chamber data. *Atmospheric Environment. Part A. General Topics*, **25 (12)**, 2771–2806.

Cazorla, M. and W. H. Brune, 2010: Measurement of ozone production sensor. *Atmospheric Measurement Techniques*, **3 (3)**, 545–555.

Cazorla, M., W. H. Brune, X. Ren, and B. Lefer, 2012: Direct measurement of ozone production rates in houston in 2009 and comparison with two estimation methods. *Atmos. Chem. Phys.*, **12 (2)**, 1203–1212.

Chen, S. and W. H. Brune, 2012: Global sensitivity analysis of ozone production and O3NOxVOC limitation based on field data. *Atmospheric Environment*, **55**, 288–296.

Chen, S., et al., 2010: A comparison of chemical mechanisms based on TRAMP-2006 field data. *Atmospheric Environment*, **44 (33)**, 4116–4125.

Cocker, D. R., R. C. Flagan, and J. H. Seinfeld, 2001: State-of-the-art chamber facility for studying atmospheric aerosol chemistry. *Environmental Science & Technology*, **35 (12)**, 2594–2601.

Czader, B. H., B. Rappenglck, P. Percell, D. W. Byun, F. Ngan, and S. Kim, 2012: Modeling nitrous acid and its impact on ozone and hydroxyl radical during the texas air quality study 2006. *Atmos. Chem. Phys.*, **12 (15)**, 6939–6951.

Derwent, R., 1990: Evaluation of a number of chemical mechanisms for their application in models describing the formation of photochemical ozone in europe. *Atmospheric Environment. Part A. General Topics*, **24 (10)**, 2615–2624.

Draxler, R. and G. Rolph, 2014: HYSPLIT (HYbrid single-particle lagrangian integrated trajectory) model access via NOAA ARL READY website. `http://www.arl.noaa.gov/HYSPLIT.php`.

Fann, N., C. M. Fulcher, and B. J. Hubbell, 2009: The influence of location, source, and emission type in estimates of the human health benefits of reducing a ton of air pollution. *Air Quality, Atmosphere & Health*, **2 (3)**, 169–176.

Finlayson-Pitts, B. J. and J. N. Pitts, 2000: *Chemistry of the upper and lower atmosphere: theory, experiments, and applications*. Academic Press, San Diego, CA.

Google, 2013: Google Maps - Houston, TX. `http://maps.google.com` Accessed: 2013-10-09.

Grell, G. A., S. E. Peckham, R. Schmitz, S. A. McKeen, G. Frost, W. C. Skamarock, and B. Eder, 2005: Fully coupled online chemistry within the WRF model. *Atmospheric Environment*, **39 (37)**, 6957–6975.

Jeffries, H., D. Fox, and R. Kamens, 1976: Outdoor smog chamber studies: Light effects relative to indoor chambers. *Environ. Sci. Technol.; (United States)*, **10:10**.

Jimenez, P., J. M. Baldasano, and D. Dabdub, 2003: Comparison of photochemical mechanisms for air quality modeling. *Atmospheric Environment*, **37 (30)**, 4179–4194.

Kleindienst, T. E., E. E. Hudgens, D. F. Smith, F. F. McElroy, and J. J. Bufalini, 1993: Comparison of chemiluminescence and ultraviolet ozone monitor responses in the presence of humidity and photochemical pollutants. *Air & Waste*, **43 (2)**, 213–222.

Kleinman, L. I., 2005: The dependence of tropospheric ozone production rate on ozone precursors. *Atmospheric Environment*, **(3)**, 575–586.

Kleinman, L. I., et al., 1997: Dependence of ozone production on NO and hydrocarbons in the troposphere. *Geophysical Research Letters*, **24 (18)**, 22992302.

Laws, E. M. and J. L. Livesey, 1978: Flow through screens. *Annual Review of Fluid Mechanics*, **10 (1)**, 247–266.

Liu, L.-J. S., I. Curjuric, D. Keidel, J. Heldstab, N. Kunzli, L. Bayer-Oglesby, U. Ackermann-Liebrich, and C. Schindler, 2007: Characterization of source-specific air pollution exposure for a large population-based swiss cohort (SAPALDIA). *Environmental Health Perspectives*, **115 (11)**, 1638–1645.

Luecken, D., S. Phillips, G. Sarwar, and C. Jang, 2008: Effects of using the CB05 vs. SAPRC99 vs. CB4 chemical mechanism on model predictions: Ozone and gas-phase photochemical precursor concentrations. *Atmospheric Environment*, **42 (23)**, 5805–5820.

Maantay, J., 2002: Mapping environmental injustices: pitfalls and potential of geographic information systems in assessing environmental health and equity. *Environmental Health Perspectives*, **110 (Suppl 2)**, 161–171.

Mao, J., et al., 2010: Atmospheric oxidation capacity in the summer of houston 2006: Comparison with summer measurements in other metropolitan studies. *Atmospheric Environment*, **44 (33)**, 4107–4115.

Martinez, M., et al., 2003: OH and HO2 concentrations, sources, and loss rates during the southern oxidants study in nashville, tennessee, summer 1999. *Journal of Geophysical Research: Atmospheres*, **108 (D19)**, 4617–4634.

Olaguer, E. P., S. C. Herndon, B. Buzcu-Guven, C. E. Kolb, M. J. Brown, and A. E. Cuclis, 2013: Attribution of primary formaldehyde and sulfur dioxide at texas city during SHARP/formaldehyde and olefins from large industrial releases (FLAIR) using an adjoint chemistry transport model. *Journal of Geophysical Research: Atmospheres*, n/an/a.

O'Neill, M. S., et al., 2003: Health, wealth, and air pollution: advancing theory and methods. *Environmental Health Perspectives*, **111 (16)**, 1861–1870.

Phoseon, 2012: Phoseon Starfire Product Datasheet. `http://phoseon.com/products/StarFire.html` Accessed: 2013-10-09.

Ren, X., et al., 2003: OH and HO2 chemistry in the urban atmosphere of new york city. *Atmospheric Environment*, **37 (26)**, 3639–3651.

Ren, X., et al., 2013: Atmospheric oxidation chemistry and ozone production: Results from SHARP 2009 in Houston, Texas. *Journal of Geophysical Research: Atmospheres*, **118 (11)**, 5770–5780.

Rohrer, F., B. Bohn, T. Brauers, D. Brning, F.-J. Johnen, A. Wahner, and J. Kleffmann, 2005: Characterisation of the photolytic HONO-source in the atmosphere simulation chamber SAPHIR. *Atmos. Chem. Phys.*, **5 (8)**, 2189–2201.

Seinfeld, J. H. and S. N. Pandis, 2006: *Atmospheric Chemistry and Physics: from air pollution to climate change*. J. Wiley, Hoboken, N.J.

Shetter, R. E. and M. Müller, 1999: Photolysis frequency measurements using actinic flux spectroradiometry during the PEM-Tropics mission: Instrumentation description and some results. *Journal of Geophysical Research: Atmospheres*, **104 (D5)**, 5647–5661.

Shetter, R. E., et al., 2003: Photolysis frequency of NO2: measurement and modeling during the international photolysis frequency measurement and modeling intercomparison (IPMMI). *Journal of Geophysical Research: Atmospheres*, **108 (D16)**, 8544–8559.

SilcoTek, 2014: SilcoTek Inert Coatings. `http://www.silcotek.com` Accessed: 2014-1-20.

Sillman, S. and P. J. Samson, 1995: Impact of temperature on oxidant photochemistry in urban, polluted rural and remote environments. *Journal of Geophysical Research: Atmospheres*, **100 (D6)**, 11 49711 508.

Spurk, J. and N. Aksel, 2008: *Fluid Mechanics*. Springer-Verlag, Berlin Heidelberg, Germany.

Stohl, A., S. Eckhardt, C. Forster, P. James, and N. Spichtinger, 2002: On the pathways and timescales of intercontinental air pollution transport. *Journal of Geophysical Research: Atmospheres*, **107 (D23)**, ACH 6–1ACH 6–17.

Texas Commissionon Environmental Quality, 2010: AQR strategic plan summary. `http://aqrp.ceer.utexas.edu/docs/AQR%20Strategic%20Plan%20Summary%20May%2027%202010.pdf` Accessed: 2013-10-13.

Thornton, J. A., et al., 2002: Ozone production rates as a function of NOx abundances and HOx production rates in the nashville urban plume. *Journal of Geophysical Research: Atmospheres*, **107 (D12)**, ACH 7–1ACH 7–17.

Tonnesen, G. S. and R. L. Dennis, 2000: Analysis of radical propagation efficiency to assess ozone sensitivity to hydrocarbons and NO x : 1. local indicators of instantaneous odd oxygen production sensitivity. *Journal of Geophysical Research: Atmospheres*, **105 (D7)**, 92139225.

US EPA, 1999: Laboratory study to explore potential interferences to air quality monitors. Govt. Doc. EP 4.52:2002006990, Office of Air Quality Planning and Standards, Research Triangle Park, NC Accessed online: 2014-01-04.

US EPA, 2010: Our nation's air - status and trends through 2010 | AirTrends | US EPA. `http://www.epa.gov/airtrends/2011/` Accessed: 2013-10-09.

Wainman, T., C. J. Weschler, P. J. Lioy, and J. Zhang, 2001: Effects of surface type and relative humidity on the production and concentration of nitrous acid in a model indoor environment. *Environmental Science & Technology*, **35 (11)**, 2201–2206.

Wilson, K. L. and J. W. Birks, 2006: Mechanism and elimination of a water vapor interference in the measurement of ozone by UV absorbance. *Environmental Science & Technology*, **40 (20)**, 6361–6367.

Zhou, Y., J. Hammitt, J. S. Fu, Y. Gao, Y. Liu, and J. I. Levy, 2013: Major factors influencing the health impacts from controlling air pollutants with nonlinear chemistry: An application to china. *Risk Analysis*, 1–15.